Title
Numerical Investigations of a Hydrogen Jet Flame in a Vitiated Coflow

Author
Frederick, Donald Jerome

Publication Date
2013

Peer reviewed|Thesis/dissertation

Numerical Investigations of a Hydrogen Jet Flame in a Vitiated Coflow

by

Donald Jerome Frederick

A dissertation submitted in partial satisfaction of the

requirements for the degree of

Doctor of Philosophy

in

Engineering – Mechanical Engineering

in the

Graduate Division

of the

University of California, Berkeley

Committee in charge:

Professor J.Y. Chen, Chair

Professor Robert Dibble

Professor Fotini Katopodes Chow

Fall 2013

Abstract

Numerical Investigations of a Hydrogen Jet Flame in a Vitiated Coflow

by

Donald Jerome Frederick

Doctor of Philosophy in Engineering - Mechanical Engineering

University of California, Berkeley

Professor J.Y. Chen, Chair

An ever increasing demand for energy coupled with a need to mitigate climate change necessitates technology (and lifestyle) changes globally. An aspect of the needed change is a decrease in the amount of anthropogenically generated CO_2 emitted to the atmosphere. The decrease needed cannot be expected to be achieved through only one source of change or technology, but rather a portfolio of solutions are needed. One possible technology is Carbon Capture and Storage (CCS), which is likely to play some role due to its combination of mature and promising emerging technologies, such as the burning of hydrogen in gas turbines created by pre-combustion CCS separation processes. Thus research on effective methods of burning turbulent hydrogen jet flames (mimicking gas turbine environments) are needed, both in terms of experimental investigation and model development. The challenge in burning (and modeling the burning of) hydrogen lies in its wide range of flammable conditions, its high diffusivity (often requiring a diluent such as nitrogen to produce a lifted turbulent jet flame), and its behavior under a wide range of pressures. In this work, numerical models are used to simulate the environment of a gas turbine combustion chamber. Concurrent experimental investigations are separately conducted (and discussed in *North* [2013]) using a vitiated coflow burner (which mimics the gas turbine environment). A variety of models are used to simulate, and occasionally guide, the experiment.

On the fundamental side, mixing and chemistry interactions motivated by a H_2/N_2 jet flame in a vitiated coflow are investigated using a 1-D numerical model for laminar flows and the Linear Eddy Model for turbulent flows. A radial profile of the jet in coflow can be modeled as fuel and oxidizer separated by an initial mixing width. The effects of species diffusion model, pressure, coflow composition, and turbulent mixing on the predicted autoignition delay times and mixture composition at ignition are considered. We find that in laminar simulations the differential diffusion model allows the mixture to autoignite sooner and at a fuel-richer mixture than the equal diffusion model. The effect of turbulence on autoignition is classified in two regimes, which are dependent on a reference laminar autoignition delay and turbulence time scale. For a turbulence timescale larger than the reference laminar autoignition time, turbulence has little influence on autoignition or the mixture at ignition. However, for a turbulence timescale smaller than the reference laminar timescale, the influence of turbulence on autoignition depends on the diffusion model. Differential diffusion simulations show an increase in autoignition delay time and a subsequent change in mixture composition at ignition with increasing turbulence. Equal diffusion simulations suggest the effect of increasing turbulence on autoignition delay time and the mixture fraction at ignition is minimal.

More practically, the stabilizing mechanism of a lifted jet flame is thought to be controlled by either autoignition, flame propagation, or a combination of the two. Experimental data for a turbulent hydrogen diluted with nitrogen jet flame in a vitiated coflow at atmospheric pressure, demonstrates distinct stability regimes where the jet flame is either attached, lifted, lifted-unsteady, or blown out. A 1-D parabolic RANS model is used, where turbulence-chemistry interactions are modeled with the joint scalar-PDF approach, and mixing is modeled with the Linear Eddy Model. The model only accounts for autoignition as a flame stabilization mechanism. However, by comparing the local turbulent flame speed to the local turbulent mean velocity, maps of regions where the flame speed is greater than the flow speed are created, which allow an estimate of lift-off heights based on flame propagation. Model results for the attached, lifted, and lifted-unsteady regimes show that the correct trend is captured. Additionally, at lower coflow equivalence ratios flame propagation appears dominant, while at higher coflow equivalence ratios autoignition appears dominant.

To Jenn and all those who've helped along they way. The list is just too large ☺

Acknowledgements

Many thanks go to Professor J.Y. Chen for his help and guidance throughout this process, the insight from Professor Robert Dibble, and of course, the experimental data collected by Andrew North was crucial to this dissertation. Additionally, many thanks go to Sintef for their support and funding.

Contents

Chapter 1

Introduction

Energy is what enables the modern world to function. From computers to transportation to food, energy (and the use thereof) is the lowest common denominator. The majority of our energy comes from fossil fuels. If it were not for the combustion of fossil fuels, the modern world would come grinding to a halt. In the United States, roughly 87% of energy is released via combustion of fossil fuel sources as of 2011 *EPA* [2013], shown in Figure 1.1. The combustion of these fossil fuels is a mixed blessing. Most, if not all, of these sources contain carbon in one form or another. Extracting energy from the carbon containing fossil fuels yields two main products: water vapor and carbon dioxide, CO_2, both of which are greenhouse gases *EPA* [2013]. While water vapor is also a greenhouse gas, it is typically not as much of concern due to its short atmospheric life-cycle *Jacobs* [1999].

Among other consequences of fossil fuel combustion, the addition of CO_2 to the environment contributes to global warming and the acidification of oceans *Caldeira* [2003]. These noticeable effects have resulted in an ongoing effort to mitigate climate change by the reduction of anthropogenic greenhouse gas emissions. Many mitigation options exist, such as energy efficiency improvements, the switch to less carbon-intensive fuels, nuclear power, renewable energy sources, the enhancement of biological sinks, as well as the reduction of non-CO_2 greenhouse gas emissions. Of the energy from fossil fuels used in the U.S., 40.1% comes from combustion in the power generation sector *EPA* [2013]. Thus focusing on reducing CO_2 emissions in the power generation sector seems prudent as it could yield significant overall reductions in CO_2 emissions. One potential route is through Carbon Capture and Storage (CCS), which is a process of capturing CO_2 from large point sources, transporting it to a storage site, and depositing it where it will not enter the atmosphere, for example, in an underground geological formation. Fossil fuel power plants are the primary application of CCS, where the CO_2 can be captured either before or after combustion, i.e. pre-combustion CCS or post-combustion CCS. The Intergovernmental Panel on Climate Change (IPCC) estimates that the economic potential of CCS could be between 10% and 55% of the total carbon mitigation effort until year 2100 *IPCC* [2005], alluding to the need for a broad scientific understanding of all processes involved.

In pre-combustion CCS, a carbon containing fuel is reformed in the first stage of reaction producing a mixture of hydrogen and carbon monoxide (syngas) from a primary fuel. There are two main routes to accomplish this. The first is to add steam (reaction 1.1), in which case the process is called steam reforming, and the other is to add oxygen (reaction 1.2) to

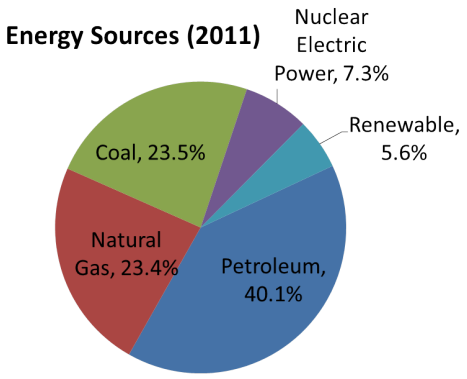

Figure 1.1: A breakdown of energy sources as detailed in *EPA* [2013].

the primary fuel, often called partial oxidation when applied to gaseous and liquid fuels and gasification when applied to a solid fuel, but the principles are the same.

Steam reforming:

$$C_xH_y + xH_2O <-> xCO + (x + \frac{y}{2})H_2 \tag{1.1}$$

Partial Oxidation:

$$C_xH_y + \frac{x}{2}O_2 <-> xCO + \frac{y}{2}H_2 \tag{1.2}$$

Reactions 1.1 or 1.2 are then followed by the water-gas shift reaction to convert carbon monoxide to CO_2 by adding steam:

Water-Gas Shift:

$$CO + H_2O <-> CO_2 + H_2 \tag{1.3}$$

where the CO_2 is then removed from the CO_2/H_2 mixture. The CO_2 can then be stored or sequestered in some manner, and the remaining H_2 sent to an end-use cycle, typically to be combined with an oxidizer and burner for energy. For power generation, the end-use is typically the combustor of a gas turbine, and thus understanding of the behavior of hydrogen combustion under gas turbine conditions is vital. One such gas turbine, and the inspiration for the work in this dissertation, is the Alstrom GT24/GT26 Sequential Combustion gas turbine (shown in Figure 1.2). The first stage of the burner is called the Environmental or EV burner (#1 in the figure). Compressed air is fed into the EV burner, creating a homogeneous, lean fuel/air mixture. The mixture is then ignited (shown at #2 in the figure), forming a low-temperature flame. The hot exhaust gases of that lean flame, which contain oxygen, exit the first combustor and move through the high-pressure turbine stage before entering the second burner (at #3 in the figure). The second burner is referred to as the Sequential Environmental (SEV) burner. In the SEV burner mixing chamber, vortex generators induce turbulence in the products of the first stage of combustion from the EV burner which enhances the upcoming mixing process with the fuel. At the fuel nozzle (#4 in the figure), hydrogen-rich fuel is injected with a carrier gas (such as Nitrogen, N_2) to delay autoignition until the mixture enters the annular SEV combustion chamber. The hot coflowing turbulent products from the first stage of combustion mix with the injected H_2-N_2 fuel, creating a partially premixed jet flame in the free space of the SEV combustor (#5

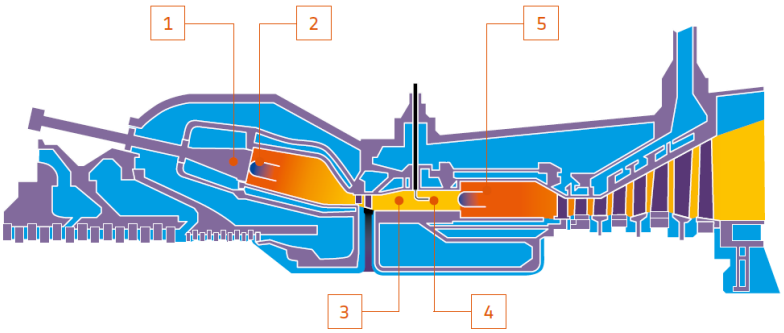

Figure 1.2: Alstrom's GT24/GT26 gas turbine.

in the figure). The hot products of the second stage of combustion then continue into the low-pressure turbine. The modeling of the physical processes of turbulence, diffusion, and chemistry occurring over a variety of pressures in the second stage of combustion will be the focus of this dissertation.

While the Alstrom turbine and general concept of combustion contained within it may be the inspiration for the research necessary to understand the physical processes, it is not feasible to work with. Thus the work contained within this dissertation is motivated by the Berkeley Vitiated Coflow Burner (VCB), which was designed to study lifted turbulent jet flames of similar characteristics to those found in industrial combustion systems such as the Alstrom GT24/GT26 turbine. Using a simplified burner such as the VCB allows study of relevant physical processes without the complexity or expense of a commercial burner. Thus although only inspired by the commercial burner, the research contained in this dissertation allows a greater and more complete understanding of the fundamental combustion processes, which can be applied to future commercial burner designs. Figure 1.3 shows a cross-sectional schematic of the VCB, which consists of a high velocity fuel jet issuing into a surrounding coflow of lean premixed hydrogen combustion products. The temperature of the coflow is controlled by its stoichiometry. Nitrogen is added to the H_2 fuel jet to increase jet momentum which encourages the flame to lift from the nozzle. The H_2 and N_2 fuel flow rates can be independently adjusted to allow for a wide possible range of jet velocities for a given amount of jet momentum. The fuel is generally at ambient temperature (roughly 300 K), while the coldest coflow is at roughly 800 K. Results from experiments conducted with the VCB (detailed in [*North*, 2013]) are used in the development and validation of the numerical models in this dissertation.

1.1 Structure of the Dissertation

The introduction given above outlines the motivation for the work contained below. The primary goal in the dissertation is to numerically investigate the fundamental phenomena occurring between mixing, turbulence, and chemistry at atmospheric to moderate pressures, and to identify dominant flame stabilization mechanisms for lifted turbulent jet flames. This is accomplished with numerical models studying the fundamental phenomena of an autoignition dominated flame. Additionally more simplified models are used to explain experimental

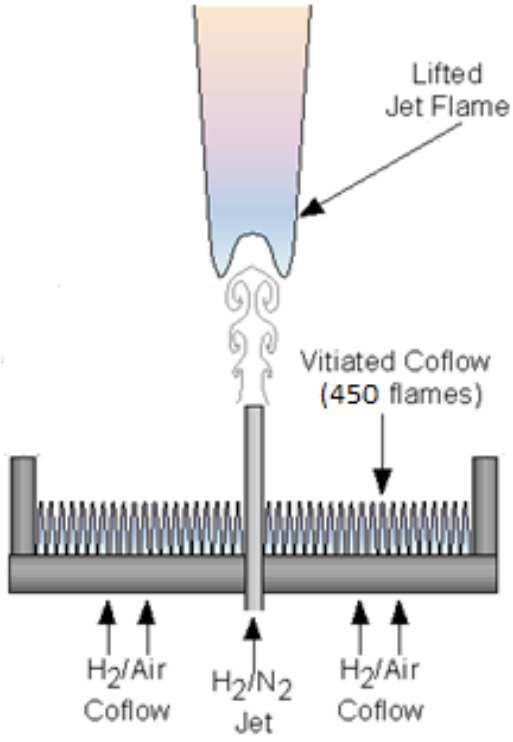

Figure 1.3: Cross section of the Berkeley Vitiated Coflow Burner (VCB), showing the configuration of coflow and central jet as well as a representation of a lifted jet flame.

trends (the data of which was collected by and is discussed in [*North*, 2013]), when autoignition cannot be the dominant flame stabilization mechanism. Chapter 2 outlines the various models used to study the Berkeley VCB. Preliminary work and literature review indicated a need for simple models to understand the physics behind a jet-in-colfow configuration. The models used throughout the dissertation are summarized and put into context for the overall goal of the research.

Chapter 3 is focused on an autoignition dominated flame and discusses the turbulence-chemistry interactions occurring on a fundamental level in a lifted jet flame, as well as the impact of the diffusion model. First, to provide some bounds on the study of mixing, homogeneously mixed autoignition delay times and mixtures at ignition are calculated. Doing so follows common practice in problems of autoignition dominated combustion events (e.g. non-premixed combustion). Generally, reference autoignition times and mixtures at ignition are taken from homogeneous calculations when studying autoignition events, thus following this common practice allows for the highlighting of possible discrepancies. Next, effects of mixing are introduced where the fuel and oxidizer are separated by a mixing layer (of variable width). This allows for the effects the mixing layer width and how the diffusion model impacts autoignition to be studied. Furthermore, impacts of N_2 dilution, scalar dissipation rate (i.e. steepness of the species gradient), and comparisons with published results are considered. Although some study of diffusion model and mixing layer width has been covered in the literature (e.g. *Knikker et al.* [2003]), it is incomplete and not fully explained. Our results indicate a need to redefine the commonly used homogeneous reference values

of autoignition delay time and mixture at ignition to account for an unmixed condition. Additionally, the results indicate the need to account for effects of differential diffusion, as differential and equal diffusion models produce different results. The chapter finishes by considering the impact of turbulence on diffusion models. Equal species diffusivity is commonly assumed in large scale models, generally with an implied assumption that turbulence can erase the effects of differential diffusion. Our results indicate that although turbulence does have an impact, its impact is similar for both equal and differential diffusion models, and thus differential diffusion effects are not erased.

Chapter 4 analyzes experimentally determined stability conditions at atmospheric pressure in the VCB and offers suggestions on stabilizing mechanisms. Experimental data (from *North* [2013]) was taken under a variety of coflow conditions, including at coflow temperatures too low to support an autoignition dominated flame. A marked change is seen in the experimentally determined stability conditions near where the coflow temperature becomes hot enough to support autoignition. This effect is investigated using a numerical model which only predicts an autoignition dominated solution, but nevertheless solves the flow field. A simple post-processing idea is used to identify regions of the flow field where the mean axial velocity is less than the turbulent flame speed. The intent is to capture the trend detailed in the stability diagrams. Laminar flame speeds are pre-calculated and a simple correlation for turbulent flame speeds - which accounts for differential diffusion effects - is used. This simple model is able to capture the trend and provide the plausible explanation that a flame stabilized in a cold coflow is done through flame propagation.

Chapter 5 concludes the present work by suggesting possible areas for future study and then presenting a final summary of numerical calculations.

1.2 Dissertation Contributions

This dissertation aims to advance the understanding of the fundamental phenomena occurring in a lifted jet flame between mixing, turbulence, and chemistry at pressures of 1-5 bar, and to identify dominant flame stabilization mechanisms for lifted turbulent jet flames. Some contributions to the overall body of science are as follows:

- Simulation of laminar autoignition for varying widths of mixing layers between fuel and oxidizer for both differential and equal species diffusion models. The results indicate a fundamentally different mixing process is occurring, leading to different autoignition delay times and different mixtures at ignition for thin mixing widths. Thick mixing widths produce a homogenous condition for both diffusion models.

- A redefinition of the autoignition reference time from a homogeneous mixture reference time to a laminar mixing reference time (for small mixing layers). Additionally, an expansion of the most reactive mixture fraction concept, to account for the wide range of reactive conditions present in hydrogen mixtures. Furthermore, a new definition of mixture fraction at ignition to account for differences in diffusion model.

- Simulation of turbulent autoignition for a fixed mixing width (of size similar to published results) for both equal and differential diffusion models. The results indicate

turbulence impacts chemistry similarly for both diffusion models and that the redefinition of reference time is needed to accurately compare to a turbulence time scale and obtain meaningful results.

- A novel and inexpensive method to determine the possibility of flame propagation as a flame stabilization mechanism in lifted turbulent jet flames. Although not exact, the method correctly captures the trends in an inexpensive manner.

Chapter 2

Background on Numerical Methods

2.1 Introduction

Numerical models aid us in understanding combustion phenomena. Combustion models range widely in goal, complexity, and scope. Direct Numerical Simulations (DNS) involve solving the fundamental equations directly and can be used as a tool to investigate fundamental processes, although DNS is computationally expensive. A more practical, or real-world, approach is to use Reynolds Averaged Navier Stokes (RANS) or Large Eddy Simulation (LES). While computationally cheaper, RANS and LES require closure models to describe the physics on a sub-grid scale level and describe the physics in an averaged sense only. Complex behavior, such as the interaction of turbulent mixing and chemistry in a lifted jet flame like the Berkeley VCB, is not well understood. Additionally, most turbulent combustion models are developed for specific regimes, such as premixed or non-premixed combustion [*Peters*, 2000]. A lifted turbulent jet flame straddles these regimes, as it is essentially a partially premixed combustion process which contains characteristics from both premixed combustion and non-premixed combustion regimes. As such, much insight can be gained through fundamental numerical modeling of the physical phenomena, which can then be used to guide sub-grid model development for RANS and LES.

Several numerical models were used in the investigation of the Berkeley VCB. These models can be broken into two essential types: models which predict autoignition, and models which predict flame propagation. Autoignition behavior was investigated using several models. The simplest was a constant pressure, adiabatic, homogeneous reactor model. Effects of laminar mixing on autoignition were investigated with a 1-D laminar mixing model, while turbulence effects on autoignition were investigated with a RANS parabolic model (referred to as the "parabolic code"), and the 1-D Linear Eddy Model. Flame propagation behavior was investigated with a 1-D laminar flame propagation model and *a posteri* with the parabolic code. For all simulations, the detailed H_2 chemical kinetic mechanism by *Li et al.* [2004] was used.

2.2 Homogeneous Reactor (Senkin)

A common practice in the modeling of a non-premixed combustion system is to bound the problem with the autoignition delay times possible for the wide variety of mixtures possible between the two unmixed streams of fuel and oxidizer (e.g. [*Hilbert & Thévenin*, 2002; *Sreedhara & Lakshmisha*, 2002; *Knikker et al.*, 2003]). Doing so gives an estimate of how long the chemistry takes to occur, as well as what mixture tends to autoignite first, and is often used as a reference in the study of more complex systems. Senkin, part of the Chemkin II software package developed at Sandia National Laboratories, contains an adiabatic, constant pressure homogeneous reactor model which is useful for predicting the time dependent chemical kinetics behavior of a homogeneous gas mixture in a closed system. Details of the model are discussed in [*Lutz et al.*, 1988]. A non-premixed system consisting of a fuel and coflow stream gives a wide variety of possible mixtures (and mixture temperatures). Assuming a perfectly mixed environment is useful as a first step in determining the minimum chemistry time necessary for autoignition to occur for a given mixture. It is additionally useful for determining the mixture composition where the minimum autoignition time takes place.

As Senkin is a homogeneous model, the autoignition delay time τ_{ign} calculated is refereed to as the Homogeneous Mixture Ignition (HMI) delay time, or τ_{HMI}. The corresponding mixture fraction occurring at $\tau_{hmi-ref}$ is called the most reactive mixture ξ_{MR}. Note these values represent mixtures that are created under the instantaneous mixing assumption and that $\tau_{hmi-ref}$ and ξ_{MR} are used as reference points in the analysis of the mixing process prior to autoignition.

2.3 One-Dimensional Mixing Model

In a non-premixed environment, mixing of some form is necessary for combustion to occur. A first step is to introduce strictly laminar (or diffusional) mixing processes. An important consideration is then how to model diffusion. Often, an equal species diffusion model is used, as doing so can greatly simplify the computational requirements. However in making the assumption that all species diffuse at the same rate, the physics of each species' diffusivity is lost and puts into question the solution accuracy. A model is only useful if the assumptions made are valid, and thus the 1-D model used allows for the study of both equal species diffusion and differential species diffusion.

The jet-in-coflow itself can be considered as essentially a radial 1-D problem at any point downstream of the jet. The computational domain is the radial coordinate (where x is the radial direction) in a spatially developing flow. Thus the time evolution along this coordinate is interpreted as spatial evolution in the stream-wise direction. At any point downstream of the jet, the fuel from the jet is separated from the oxidizer of the coflow by a gradient, referred to as initial mixing width, d. Therefore, given initial scalar profiles which represent a fuel and oxidizer stream a certain distance downstream, a 1-D mixing model can be used to solve the scalar fields of temperature and species composition. A schematic of the model is shown in Figure 2.1. The model is formulated in terms of the following species and energy

equations for the evolving scalar fields $Y_i(x,t)$ and $T(x,t)$ according to

$$\rho\frac{\partial Y_i}{\partial t} = -\frac{\partial(\rho V_i Y_i)}{\partial x} + M_i\dot{\omega}_i \tag{2.1}$$

$$\rho\overline{c_p}\frac{\partial T}{\partial t} = -\sum_{i=1}^{K_s} c_{p_i} Y_i V_i \frac{\partial T}{\partial x} + \frac{\partial}{\partial x}\left(k\frac{\partial T}{\partial x}\right) - \sum_{i=1}^{K_s} h_i M_i \dot{\omega}_i \tag{2.2}$$

where

$$V_i = -\frac{D_i}{Y_i}\frac{\partial Y_i}{\partial x} \tag{2.3}$$

$$\rho = \frac{PM_i}{T\sum_{i=1}^{K_s} Y_i R_u} \tag{2.4}$$

and D_i is the molecular diffusivity of each species, T is the temperature, ρ is density, M_i is the molar mass, $\dot{\omega}_i$ is the reaction rate, h_i is the enthalpy, k is the thermal conductivity, c_p is the specific heat, V_i is the diffusion velocity, and K_s is the number of species.

The species diffusion is simplified in terms of the Lewis number, $Le_i = \alpha/D_i$, which is held constant for each species throughout the simulation. By using the Lewis number formulation, considerable computational savings are achieved over a full multicomponent diffusion model. For equal diffusion calculations, all species Lewis numbers are set to unity. However, for differential diffusion calculations, unique Lewis numbers are assigned to each species, which are calculated *a priori* using Chemkin. A full multicomponent model is also used for validation of the simpler Lewis number formulation, results of which are discussed in Section 3.4.4. Unless otherwise noted, "equal diffusion model" and "differential diffusion model" refer to the simpler Lewis number formulation.

To smooth the interface between hot oxidizer and cold fuel, the mixture fraction (ξ) profile is initialized according to

$$\xi = \frac{1}{2}\left(1 + \text{erf}\left(\frac{x - x_0}{d}\right)\right) \tag{2.5}$$

where d is the initial mixing width as previously mentioned and the error function is used to create a smooth gradient. Equal diffusion is assumed to initialize the mixing width profile, after which either an equal or differential species diffusion model is applied, so that the effects of the diffusion model can be directly observed. It must be noted that in the simulations by *Knikker et al.* [2003], their initialization of d allows for a bulk initial mixing width with separate profiles in the initial mixing width of H_2 and O_2, which are based on an averaged Lewis number for each species [*Knikker et al.*, 2003].

2.4 The Linear Eddy Model

In an ideal world, CFD simulations would all be done as DNS where all scales of turbulence are resolved. However, resolving all scales in three-dimensional CFD requires computational power that makes simulation of practical applications untenable. But all is not lost, and although it may be untenable to fully resolve all scales in a turbulent flow all the time, it is

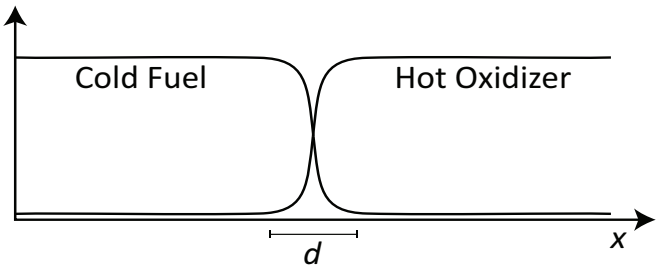

Figure 2.1: Initial mixing width definition and schematic of the 1-D mixing model.

still quite possible to study the effects of turbulence and chemistry in a simpler sense. One such method, called the Linear Eddy Model (LEM) [*Kernstein*, 1988a], is a one dimensional formulation which models turbulent stirring and is essentially an extension of the 1-D mixing model introduced above to include turbulence. Instead of directly solving the Navier-Stokes equations in 3-D, the main idea of the LEM is to model turbulent stirring by random spatial rearrangement events of the scalar field while resolving all relevant length and time scales. The LEM is based on a stochastic model of fluid motion derived from statistical scaling laws for turbulence. Although turbulence is inherently 3-D, convective stirring is replaced by a simplified representation of eddy motions in 1-D.

In the LEM, as with the 1-D laminar mixing model, the computational domain is the radial coordinate in a spatially developing flow. Thus the time evolution along this coordinate is interpreted as spatial evolution in the stream-wise direction, in other words, as the flow moves downstream from the jet. Each stirring event is seen as the action of an individual eddy [*Kernstein*, 1988a,b]. The stirring (or rearrangement process) is simulated with a block-inversion model, called triplet mapping, the details of which are discussed below. Aside from the triplet mapping, the Linear Eddy Model makes no other approximations on the molecular diffusion or chemical reactions. As with the 1-D laminar mixing model, equal species diffusivity or differential species diffusivity can be simulated. Due to the one-dimensional nature, full resolution of all relevant length scales is possible, from the Kolmogorov scale η, to the integral scale l_0 [*McMurty et al.*, 1993]. These unique features make the LEM an ideal platform to study the impact of turbulent stirring on chemical reactions in a turbulent environment such as the Berkeley VCB.

As turbulence is inherently a three-dimensional phenomena [*Pope*, 2000], the LEM focuses on two key mechanisms in the turbulent flows: molecular diffusion and turbulent convection. Turbulent eddies are theorized to enhance diffusion by steepening scalar gradients [*Pope*, 2000]. Thus, the LEM mimics eddies by steepening scalar gradients, where the effect of a single eddy in a one-dimensional scalar field can be visualized in Figure 2.2. The size of the eddy and the frequency of the stirring are selected in a stochastic manner to mimic the overall turbulent stirring within a given turbulence spectrum. The eddy stirring process itself is modeled with a triplet map. The triplet map first creates three copies of a selected segment and then steepens the gradients of the copies by a factor of three by compressing the spatial range. The copies are aligned next to each other and the middle copy is spatially reversed. The original selected segment is then replaced by the newly mapped segment, where molecular diffusion smooths the discontinuous regions. The process is illustrated in

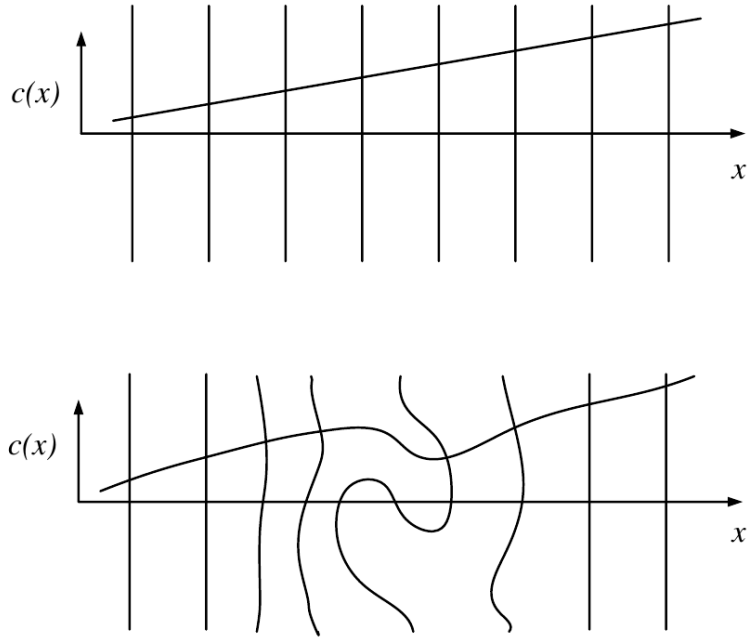

Figure 2.2: A linear scalar field mixed by the Linear Eddy Model. Vertical lines are used to illustrate the effect of an eddy stirring the scalar field from unmixed (top) to mixed (bottom).

Figure 2.3.

Three variables control each stirring event (triplet map): the location of the stirring, the stirring event rate, and the size of the affected segment (eddy). The triplet map location is determined randomly from a uniform distribution within the spatial 1-D domain. The stirring event rate is given by $E = \lambda X_{LEM}$, where X_{LEM} is the domain length and the event frequency λ is determined from *Kernstein* [1991]

$$\lambda = \frac{54}{5}\frac{\nu Re_t}{C_\lambda l_0^3}\frac{(l_0/\eta)^{5/3}-1}{1-(\eta/l_0)^{4/3}} \tag{2.6}$$

where the model constant $C_\lambda = 2$. The segment (eddy) size is determined randomly from a Probability Density Function (PDF) of eddy sizes in the range between η and the integral length scale l_0, given by

$$f(l) = \frac{5}{3}\frac{l^{-8/3}}{\eta^{-5/3}-l_0^{-5/3}} \tag{2.7}$$

in the range of $\eta < l < l_0$.

The reactive flow formulation was adopted from the study by *Smith & Menon* [1997]. In a one-dimensional spatial domain, the species and temperature equations representing molecular transport and chemical reaction which describe the evolution of a constant pressure scalar field $Y(x,t)$ are the same as those presented above for the 1-D mixing model. The numerical grid is spatially resolved to at least 1/6 of the Kolmogorov length scale and is

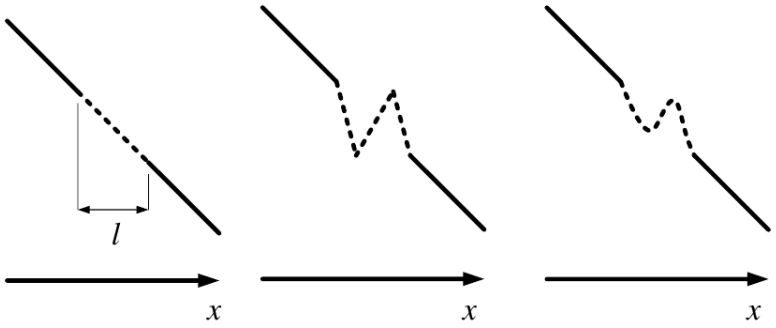

Figure 2.3: An illustrative process of the triplet map. A PDF determines the eddy size, l, sampled (first image). The segment is then compressed by a factor of three, and mirrored twice to fill the original segment length of l (second image). Molecular diffusion then smooths the resultant "zig zag" seen in the second image to produce the stirred section (third image).

related to the turbulent Reynolds number, Re_t by,

$$\eta = l_0 Re_t^{-3/4} \tag{2.8}$$

Estimates of Re_t are obtained from a 1-D RANS PDF combustion model [*Chen & Kollmann*, 1989], which is used to simulate jet flames similar to those created by the VCB, the details of which are discussed in Section 2.6. By varying the jet Reynolds number Re_j, the input parameters for turbulent LEM simulations (such as the velocity fluctuation, u') are estimated from the PDF model. As with the 1-D laminar mixing model, the species diffusion is again simplified in terms of the Lewis number, $Le_i = \alpha/D_i$, which is held constant for each species throughout the simulation. For equal diffusion calculations, all species Lewis numbers are set to unity. However, for differential diffusion calculations, unique Lewis numbers are assigned to each species, which are calculated *a priori* using Chemkin. Again, a full multicomponent diffusion model including thermal diffusion was also tested for consistency, with similar results to the simple Lewis number formulation with non-unity Lewis numbers (with results shown in section 3.4.4. A detailed hydrogen chemical kinetic mechanism developed by *Li et al.* [2004], is used for all computations.

2.5 Transient Flamelet Model

Steady flamelet models have been developed to model both premixed and non-premixed combustion regimes, and rely on pre-tabulation of chemistry. The general idea behind all flamelet models is the separation of the chemistry solution from the numerical solution of the turbulent flow and mixture fields. The premixed vs. non-premixed model formulations vary based on assumptions inherent in the combustion regime, and steady tabulated models cannot accurately account for transient effects or high turbulence [*Peters*, 2000]. To account for transient effects, transient flamelet models have been developed which do not tabulate chemistry but instead calculate on the fly, making them expensive as RANS or LES combustion

models [*Peters*, 2000]. Transient flamelet models are generally used to model non-premixed turbulent flames, and are thus useful in the case of a (non-premixed) jet flame. A conserved variable is chosen that describes the local mixture (the mixture fraction, ξ), and transport equations for the moments of a conserved variable are solved. Turbulent mean values of the mass fractions of chemical components can then be calculated by using a presumed PDF of the mixture fraction, whose shape is determined by its statistical moments [*Pitsch et al.*, 1998]. Aside from the PDF, the only requirement of the model is that locally, there exists a unique relation between the mixture fraction and all scalar quantities, such as the species mass fractions and the enthalpy. The advantage of the model is that it includes both finite-rate chemistry and the influence of the local mixture fraction gradients imposed by the flow field, i.e. the scalar dissipation rate, χ.

The transient flame model can also be used to obtain estimates of the critical scalar dissipation rate χ_{crit}, beyond which autoignition does not occur in a practical amount of time. This is crucial for a discussion of how scalar dissipation rate (i.e. turbulent stirring) impacts autoignition and is very difficult to otherwise estimate with a model such as LEM. However, the formation of the flamelet model (see below) allows for estimates of the critical scalar dissipation rate by specifying a desired mixture fraction and temperature and then step-wise increasing the scalar dissipation rate until autoignition no longer occurs. The estimates of χ_{crit} are not expected to be an exact value when compared to χ obtained from the other models (i.e. 1-D laminar mixing and LEM), but are used as relative guidance. However, an important distinction is that the standard flamelet equations are not used, as they do not allow for differential diffusion. Instead, we follow *Pitsch & Peters* [1998] to account for differential diffusion. The flamelet equations take the form,

$$\rho\frac{\partial Y_i}{\partial t} = \frac{\rho\chi Le_\xi}{2Le_i}\frac{\partial^2 Y_i}{\partial \xi^2} + M_i\dot{\omega}_i + extra\ terms \tag{2.9}$$

and

$$\rho\frac{\partial T}{\partial t} = \frac{\rho\chi}{2}Le_\xi\frac{\partial^2 T}{\partial \xi^2} + \frac{1}{c_p}\frac{\partial p}{\partial t} - \sum_{i=1}^{K_s} h_i M_i\dot{\omega}_i + extra\ terms \tag{2.10}$$

where Le_ξ is the Lewis number mixture fraction, and the extra terms account for the additional effects of differential diffusion (detailed in *Pitsch & Peters* [1998]). The above model reduces to the standard flamelet equations when unity Lewis numbers (i.e. equal diffusivities) are assumed.

2.6 Probability Density Function Combustion Model (Parabolic Code)

The probability density function (PDF) combustion model, referred to as the "parabolic code" due to the nature of the solution, is a 1-D RANS model developed to solve a jet-in-coflow problem. This model is useful to obtain quick estimates of the flow field and was validated for autoignition in previous jet-in-coflow studies ([*Cabra*, 2002, 2003]). When compared to large scale RANS or LES such as Fluent or OpenFOAM, the parabolic code

is an attractive yet much less expensive model, as it takes advantage of the axis-symmetric geometry of the flame. Additionally, previous studies indicate the additional expense of a 2-D or 3-D RANS model in Fluent provides the same results as the parabolic code [*Frederick*, 2010]. The model utilizes the joint scalar PDF for composition only and the k-ϵ turbulence model for a parabolic flow [*Smith et al.*, 1995]. The model was originally developed in the late 1980s by *Chen & Kollmann* [1989], and for mixing, originally used the gradient diffusion model and the Curl mixing model [*Pope*, 1990] to simulate the turbulent flux and scalar dissipative terms appearing in the PDF transport equation respectively. For the work in this dissertation, mixing is modeled with the Linear Eddy Model [*Chen & Kollmann*, 1999]. The Monte Carlo simulation technique is used to compute the transport equation for the PDF [*Chen & Kollmann*, 1989]. *Pope* [1981] has shown that the convergence rate of the statistics deduced from the Monte Carlo simulation is proportional to the square root of the number of representations used. Consequently, a large number of statistical representations (commonly referred to as particles) are needed to achieve accurate solutions; we typically use 400 particles per grid cell. Four hundred stochastic particles per grid cell proved a balance between accuracy of the solution (checked against more particles) and speed of computation. A detailed hydrogen chemical kinetic mechanism by *Li et al.* [2004] is again used, as well as equilibrium coflow temperatures.

In essence, the parabolic code solves a 1-D radial problem while marching downstream. Thus, flame propagation calculations are not possible (as a flame should be allowed to propagate upstream) and only autoignition is predicted. However, a simple concept and correlation using the laminar flame speed is used to give estimates of where a flame might exist once the flow field is solved, which is discussed in the following section.

2.7 Premix and Parabolic Code Post Processing

Essential to any discussion of turbulent flame propagation is the laminar flame speed, S_L. This largely hinges on a common assumption that laminar flame speed and turbulent flame speed are in some manner linked [*Warnatz et al.*, 2006], commonly with correlations relating the two for various conditions. A FORTRAN code called Premix developed at Sandia National Laboratories and part of the Chemkin package, models adiabatic freely propagating 1-D laminar premixed flames, and enables the determination of flame speeds under a wide range of conditions [*Kee et al.*, 1985]. The solutions are useful not only to study chemical kinetics in flames but also as a tool to evaluate stabilization mechanisms for lifted flames. As with the homogeneous autoignition calculations, a large range of possible mixtures exist in the jet-in-coflow configuration. Thus, laminar flame speeds for that large range of mixtures are calculated with Premix for global equivalence ratios ranging from roughly $0.4 < \phi < 2.5$. The computed laminar flames speeds are then fit to the form,

$$S_L(\phi) = a\phi^b e^{-c(\phi - d)} \tag{2.11}$$

where the coefficients a, b, c, and d are functions of N_2 fuel dilution.

As mentioned above, often laminar flame speeds are used in correlations or models of turbulent premixed flame speed and turbulent triple flame speed. One such model for turbulent

flame speed, S_T presented by *Muppala et al.* [2007] is

$$\frac{S_T}{S_L} = 1 + \frac{0.46 Re_t^{0.25}}{e^{Le-1}} \left(\frac{u'}{S_L} \right)^{0.3} \tag{2.12}$$

where Le is the mixture Lewis number and u' is the local turbulent fluctuating velocity. The turbulent Reynolds number is defined in terms of the local turbulence length scale, l and kinematic viscosity, ν as $Re_t = u' l_0 / \nu$. This correlation is chosen above all others as it additionally accounts for the Lewis number of the mixture (in addition to the hydrodynamics) and hence incorporates differential diffusion effects. Starting with a precomputed solution of a jet-in-coflow from the parabolic code, additional post-processing is applied to determine regions within the jet and surroundings where a flame might be stable or anchored. In other words, by comparing the local turbulent flame speed (S_T) to the local turbulent mean axial velocity ($\bar{U}$), maps of regions where S_T is greater than the flow speed are created, indicating where a turbulent premixed propagating flame is possible. Results are discussed in Chapter 4.

Chapter 3

Chemistry, Diffusion, and Turbulence Effects on Autoignition

3.1 Introduction

The autoignition of a fuel jet into a hot turbulent coflow is a problem of theoretical and practical interest, because of the fundamental interactions among chemical reactions, molecular diffusion, and turbulent transport and the applications to gas turbines. However, autoignition of a fuel-oxidizer mixture is possible only if temperatures are above the autoignition temperature. The autoignition temperature of hydrogen in quiescent air is roughly 800 K [*Patnaik*, 2007]. A coflow temperature of $T_{coflow} = 800$ K is equivalent to an experimental coflow equivalence ratio $\phi_{coflow} = 0.2$. Heat losses in the experiment allow for a higher coflow equivalence ratio than that predicted by equilibrium chemistry. Meaning, assuming equilibrium chemistry with no heat losses, $T_{coflow} = 783$ K when $\phi_{coflow} = 0.15$. Thus the experimental result is used to guide the model, and coflow temperatures below 800 K are not expected to be within the autoignition regime.

The definition of the autoignition delay time is quite important. Autoignition itself is dependent on local conditions such as the mixture temperature, composition, scalar dissipation rate χ, and pressure. In previously published results, the autoignition delay time has been defined for DNS (e.g. *Hilbert & Thévenin* [2002] and *Knikker et al.* [2003]) using the heat release rate (where q is heat), as

$$\frac{dq}{dt}|_{t=t_{ign}} = 0 \tag{3.1}$$

or

$$\frac{d^2q}{dt^2}|_{t=t_{ign}} = 0 \tag{3.2}$$

Another possibility is to define autoignition as the time at which the marker variable, such as H, reaches the maximum temporal gradient (e.g. *Im et al.* [1998]). However, these definitions become problematic for turbulent Linear Eddy Model (LEM) simulations and sometimes incorrectly predict autoignition. The LEM is a stochastic model that can generate large gradients when a stirring event occurs, making it difficult to use any form of gradient as a

criteria for defining autoignition. Therefore, autoignition is instead defined as the time when the local temperature of the mixture reaches the average of the local equilibrium temperature and initial mixture temperature, i.e. about 50% of the heat release. The mixture fraction for all models is calculated using the deficient species (hydrogen) [*Warnatz et al.*, 2006], as one expects autoignition to occur in lean mixtures (due to higher energy contained in the coflow side).

Two-dimensional Direct Numerical Simulations (DNS) have demonstrated the existence of a most reactive mixture fraction ξ_{MR} [*Mastorakos*, 2009], around which a mixture is most likely to autoignite at low χ (i.e. where the mixture is nearly homogeneous). Often homogeneous mixture ignition (HMI) calculations are used to determine the minimum autoignition delay time around ξ_{MR}. Using HMI calculations, ξ_{MR} and a reference autoignition delay time $\tau_{hmi-ref}$, can be calculated *a priori* [*Knikker et al.*, 2003].

HMI calculations assume an initially perfectly mixed environment (i.e. homogeneous) where radical build up and thermal runaway can occur, leading to autoignition. In practice, when fuel and oxidizer streams are not premixed, HMI calculations do not account for the initial transport processes required prior to autoignition, as noted by *Knikker et al.* [2003] and *Mastorakos* [2009]. Species transport requires a finite amount of time and the resulting τ_{ign} and mixture fraction at ignition ξ_{ign} can be quite different than those based on instantaneous mixing (i.e. HMI). The review paper by *Mastorakos* [2009] emphasizes the role of scalar dissipation rate on the propensity of a mixture to autoignite. Specifically, regions of high χ can locally delay the reactions (and hence autoignition) due to heat and radical species loss. For autoignition to occur, χ must be below a critical value for a period of time long enough for species and temperature to accumulate, and thus the local history of χ is important. *Im et al.* [1998] show that for low and moderate turbulent intensities, τ_{ign} appears insensitive to turbulence. However, for stronger turbulence, autoignition is slightly retarded due to a high initial χ. *Hilbert & Thévenin* [2002] demonstrate with 2-D DNS that the effect of turbulent Reynolds number Re_t on τ_{ign} is also very small, but that turbulent flames always ignite faster than laminar ones. *Sreedhara & Lakshmisha* [2002] use the turbulence timescale τ_{turb} to define two turbulent regimes from a turbulent 3-D DNS. The first regime is defined by $\tau_{hmi-ref} > \tau_{turb}$, where mixing is the rate-limiting process and hence τ_{ign} is influenced by τ_{turb}. The second regime is defined by $\tau_{hmi-ref} < \tau_{turb}$, where autoignition is dominated by kinetics and therefore turbulence has little effect.

When molecular diffusion plays an important role in the overall mixing processes (such as when the fuel consists partially of hydrogen) the choice of diffusion model becomes crucial. While an equal species diffusivity model is a simple starting point, the effects of hydrogen's high diffusivity on autoignition delay cannot be properly accounted for. *Knikker et al.* [2003] used one-dimensional calculations to show that laminar mixing delays the ignition process, but that the high diffusivity of hydrogen counterbalances for this delay. Additionally, when the flow is turbulent, hydrogen transport due to molecular diffusion may be of the same order as turbulent transport.

This section investigates the effects of species diffusion models for both laminar and turbulent mixing conditions on τ_{ign} and ξ_{ign} for a non-premixed H_2/N_2 jet flame in a vitiated coflow of two compositions. Moreover, the effect of pressure on τ_{ign} and ξ_{ign} is also investigated. For laminar calculations, a wide range of initial mixing widths are investigated, while for turbulent calculations, the initial mixing width is fixed and a wide range of turbulent

		Burner Environment 1	Burner Environment 2
jet	T_{jet} [K]	325	300
	% H_2 in fuel	30	30
coflow	T_{coflow} [K]	1045	1200
	ϕ_{coflow}	0.27	0.35
	% O_2	14.74	12.63
	% H_2O	9.89	13.67
	% N_2	75.34	73.51
	ξ_{st}	0.4185	0.3870

Table 3.1: Simulation parameters for both burner environments.

Reynolds numbers Re_t are investigated. The main simulations are performed using a fuel jet consisting of 30% H_2 with 70% N_2 by volume. Additionally, a more appropriate autoignition reference time based on laminar results, $\tau_{lam-ref}$ is discussed. The reference time is obtained by using laminar mixing calculations rather than HMI calculations, as HMI calculations prove inadequate in a non-premixed system such as this.

3.2 Conditions

Two variations in burner environment are simulated, for pressures of 1, 2, and 5 bar. In the first burner environment, we set the coflow temperature T_{coflow} and jet temperature T_{jet} to 1045 K and 325 K respectively, mirroring the experimental conditions of *Cabra* [2003]. The first burner environment corresponds to a coflow equivalence ratio, $\phi_{coflow} = 0.27$, with associated species concentrations and an overall stoichiometric mixture fraction, $\xi_{st} = 0.4185$. In the second burner environment, $T_{coflow} = 1200$ K and $T_{jet} = 300$ K, mirroring an upper bound of ongoing experiments. The second burner environment corresponds to a coflow equivalence ratio, $\phi_{coflow} = 0.35$, with associated species concentrations and an overall ξ_{st} = 0.3870. The coflow flame itself is not simulated, rather only the products of a premixed flame are used as input conditions for the coflow. The coflow composition is calculated using the relation given by *Cabra* [2003], and is shown, along with simulation parameters, in Table 3.1. An additional simulation with pure H_2 as the fuel in burner environment 2 at a pressure of 2 bar is used to illustrate the effects of N_2 dilution.

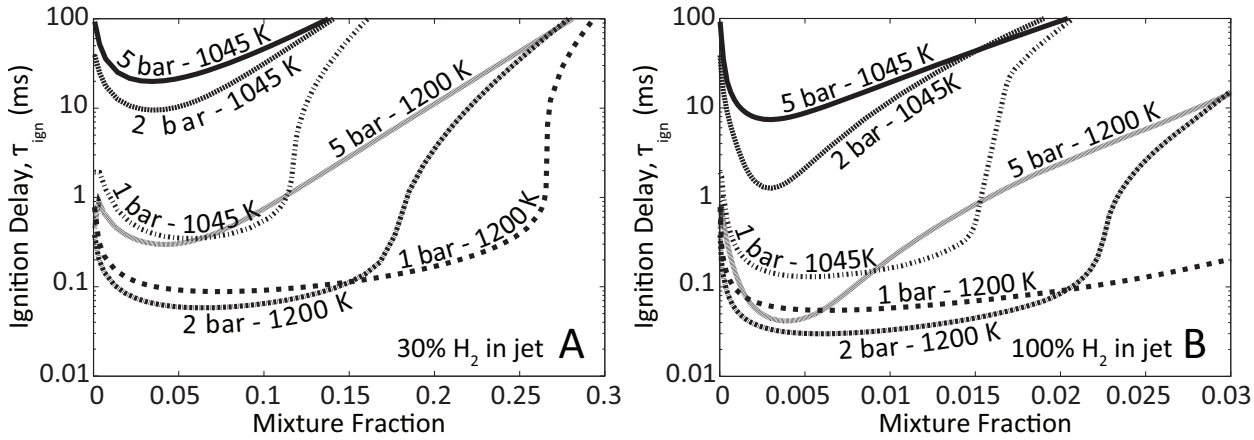

Figure 3.1: Autoignition delay times for homogeneous mixtures in burner environments 1 and 2 at pressures of 1, 2, and 5 bar. Plot A is for a fuel of 30% H_2 and 70% N_2, while plot B is for a fuel of 100% H_2. The autoignition properties are highly dependent on the mixture composition, burner pressure, and the coflow temperature.

3.3 Homogeneous Mixtures

The HMI calculations presented here assume a composition of fuel and oxidizer that is mixed instantaneously. In practice, a gradient between fuel and oxidizer streams exists, which takes a finite amount of time to relax by transport processes. In the following sections, we investigate the effects of species diffusion model, when the fuel and oxidizer are not premixed, meaning an initial gradient (characterized by d) exists. However, HMI calculations are performed as a baseline to obtain the minimum autoignition delay time ($\tau_{hmi-ref}$) and corresponding ξ_{MR}, to be used as reference values in subsequent sections. A similar approach is followed by *Knikker et al.* [2003]. Figure 3.1A shows the calculated autoignition delay times versus mixture fraction for homogeneous mixtures in both burner environments at pressures of 1, 2, and 5 bar. Figure 3.1B shows the same quantities but for 100% H_2 in the jet. Under some burner environments and pressure combinations, the autoignition delays have a broad span of mixture fraction space over which the minimum autoignition delay remains roughly constant, as seen in Figure 3.1. Therefore, we also define a most reactive mixture fraction range, where the autoignition delay time is within 10% of the minimum, a notable difference from the approach followed by *Knikker et al.* [2003] where they only were concerned with ξ_{MR} and not a range of ξ_{MR}. The percentage chosen is somewhat arbitrary and serves as a guide to illustrate the range of mixtures which autoignite at roughly the same time. For example, at atmospheric pressure in burner environment 1, a minimum autoignition delay time of $\tau_{hmi-ref} = 0.347$ ms is found at $\xi_{MR} = 0.0544$. Additionally, the most reactive mixture fraction range is $0.0414 < \xi_{MR} < 0.0671$. All the results are summarized in Table 3.2. As expected, $\tau_{hmi-ref}$ displays a very high sensitivity to T_{coflow} and pressure. In general, increasing pressure decreases the range of ξ_{MR}, while increasing the coflow temperature increases the range of ξ_{MR}. Furthermore, the homogeneous mixtures always autoignite leaner than the stoichiometric mixture fraction ξ_{st} due to the high temperature of the hot oxidizer. We will discuss and refer to these results later in the dissertation.

Pressure	1045 K coflow			1200 K coflow		
[bar]	$\tau_{hmi-ref}$ [ms]	ξ_{MR}	ξ_{MR} range			
	$\tau_{hmi-ref}$ [ms]	ξ_{MR}	ξ_{MR} range			
1	0.347	0.0544	0.0414 - 0.0671	0.088	0.0704	0.0423 - 0.1121
2	9.51	0.0347	0.0280 - 0.0480	0.058	0.0594	0.0423 - 0.0918
5	19.9	0.0347	0.0211 - 0.0480	0.297	0.0423	0.0306 - 0.0538

Table 3.2: Autoignition delay for homogeneous mixtures for various coflow temperatures and pressures. The fuel is 30% H_2 diluted with 70% N_2. The autoignition properties are highly dependent on the mixture composition, burner pressure, and the coflow temperature.

		Burner Environment 1 (1045 K Coflow)		Burner Environment 2 (1200K Coflow)	
	Diffusion Model	eq	dd	eq	dd
χ_{crit} [1/s]	1 [bar]	1700	1800	6690	8100
	2 [bar]	31	210	11200	10500
	5 [bar]	14	38	1000	4300
	2 [bar] 100% H_2 jet	–	–	618	107

Table 3.3: Critical scalar dissipation rates for the simulations performed.

3.3.1 Critical Scalar Dissipation Rate

It has been shown that autoignition occurs in regions of low scalar dissipation rate and that a critical scalar dissipation rate, χ_{crit}, exists beyond which no autoignition occurs [*Mastorakos*, 2009]. To obtain an estimate of χ_{crit} we use the aforementioned transient flamelet model to specify χ (described briefly in Section 2.5 and in much detail by *Pitsch & Peters* [1998]). χ is continually increased until autoignition no longer occurs, at which point we define $\chi = \chi_{crit}$. For values of $\chi > \chi_{crit}$, autoignition does not occur in a finite time. Results for 100% hydrogen as well as the two burner environments and all pressures investigated are presented in Table 3.3. Unity Lewis number simulations are denoted with "eq", while the differential diffusion model is denoted with "dd". Comparing χ_{crit} to $\tau_{hmi-ref}$, it is seen that χ_{crit} decreases with increasing $\tau_{hmi-ref}$. Thus, mixtures which have a tendency to autoignite quickly have a higher resistance to the mixing processes than mixtures which take longer to autoignite.

3.4 Laminar Mixing

d Flame (P For a laminar diffusional process, species transport by molecular diffusion is the only mechanism responsible for relaxing initially high scalar gradients between fuel and oxidizer streams. Autoignition occurs only when suitable conditions are created through the transport and mixing of fuel and oxidizer. Thus autoignition is expected to be dependent on d and χ, as well as the amount of diluent (such as N_2) present in the fuel. In the following sections, we examine the effects of d, χ, and N_2 dilution on τ_{ign} for equal and differential diffusion models.

3.4.1 Initial Mixing Width

When d is sufficiently large (and the species gradient $\frac{\partial Y_i}{\partial x}$ is small), little diffusive flux occurs across the mixing width prior to autoignition since chemical reactions are faster than transport processes. In this case, χ is low and conditions resemble those of a homogeneous mixture. Therefore, it is expected that both the equal diffusion and differential diffusion models approach the homogeneous limit, i.e. $\tau_{hmi-ref}$ and ξ_{MR}. In other words, as the mixture approaches the homogeneous limit (e.g. when d is large and χ is small), the effects of differential diffusion are muted and the diffusion model chosen is unimportant.

However, much smaller mixing widths (and much higher scalar gradients) are encountered for a jet issuing into a coflow such as the VCB. At small initial mixing widths, the large initial gradients in species composition and temperature will drive a strong diffusive flux (high scalar dissipation rate), as transport by molecular diffusion is the primary mixing mechanism. Due to hydrogen's high mass diffusivity relative to other species, at small initial mixing widths an equal diffusion model will incorrectly estimate transport and hence τ_{ign} and ξ_{ign}. Therefore, a differential diffusion model, which captures hydrogen's high mass diffusivity, will differ from an equal diffusion model in mixture fraction evolution, leading to variations in τ_{ign} and ξ_{ign} between models.

Figure 3.2 presents autoignition delay times computed for a mixture consisting of a fuel of pure H_2 at a temperature of 300 K in burner environment 2 (1200 K coflow). Nitrogen dilution will be considered in a later section. Computed τ_{ign} as a function of d for both equal and differential diffusion models are shown in Figure 3.2A, while Figure 3.2B presents the mixture fraction at ignition, ξ_{ign} as a function of d. As expected, at large d, both τ_{ign} and ξ_{ign} for each model asymptote to the homogeneous limit. Thus for large d, the diffusion model chosen is unimportant. However at small d, both diffusion models autoignite later than the HMI model predicts. Additionally, the differential diffusion model autoignites much richer than the equal diffusion model. This is because the mixture fraction is based on the deficient species (i.e. H_2). The differential diffusion model allows H_2 to rapidly diffuse into the oxidizer which, as the products of lean premixed combustion, contains H_2O. The H_2O has a slightly lower Lewis number than the other major species of N_2 and O_2, and can diffuse more rapidly. Thus ξ_{ign} for differential diffusion always appears richer than for equal diffusion, which is consistent with *Hilbert & Thévenin* [2002].

The computed results differ from those of *Knikker et al.* [2003] and are discussed in Section 3.4.5. However, while we initialize d assuming equal diffusion in the case of both diffusion models, their initialization of d allows for a different initial mixing width of H_2 compared to

O_2, as previously mentioned (Section 2.3). Thus, it is reasonable that a different solution is reached, as the initial conditions are vital to the final solution.

Similar to a reference time being defined for homogeneous simulations, in the limit of small initial mixing widths, we define a laminar autoignition delay time based on diffusion model, i.e. $\tau^{dd}_{lam-ref}$ and $\tau^{eq}_{lam-ref}$ where "dd" refers to differential diffusion and "eq" refers to equal diffusion. Analogous to $\tau^{dd}_{lam-ref}$ and $\tau^{eq}_{lam-ref}$, $\xi^{dd}_{lam-ref}$ and $\xi^{eq}_{lam-ref}$ are also defined. These reference times provide a benchmark for the turbulent simulations, discussed later in Section 3.5, as turbulent mixing can create sharp gradients.

3.4.2 Scalar Dissipation Rate

For thin initial mixing widths ($d \lesssim 0.1mm$), the initially high scalar gradients create large scalar dissipation rates, which can delay autoignition. As shown in the previous section, for a fuel of pure H_2, at small d both diffusion models autoignite later than the HMI model predicts, and τ_{ign} differs markedly between diffusion models. Results for the 100% H_2 fuel simulation are presented in Figure 3.3A, where it can be seen that χ_{crit} for differential diffusion is 107 s^{-1}, while for equal diffusion it is 618 s^{-1}, or roughly six times larger. By examining the time history of χ from the 1-D model at ξ_{ign} (presented in Figure 3.3B), it is seen that χ starts high and decays as expected. The differential and equal diffusion models start at different initial scalar dissipation rates because of differing ξ_{ign} being tracked. For equal diffusion, χ starts below χ_{crit}, yet takes longer to ignite than the differential diffusion model. The differential diffusion model, which starts with χ higher than χ_{crit} is still able to ignite sooner than the equal diffusion model. As previously noted, the 1-D mixing model and the flamelet model are different, however insight from both can still be provided. The trend seen in the flamelet model for low χ shows (in Figure 3.3A) that for the equal diffusion model, $\tau_{ign} \approx 0.2$ ms, which is roughly four times that of the differential diffusion model where $\tau_{ign} \approx 0.05$ ms. Thus, with consideration of τ_{ign} for respective diffusion models, it seems reasonable that the differential diffusion model ignites sooner than the equal diffusion model despite starting with a higher initial χ.

3.4.3 N_2 Dilution

We will now consider the effects of N_2 dilution on the fuel stream. The effect of fuel N_2 is expected to be most pronounced in HMI and equal diffusion computations as the mixture at ignition contains large quantities of N_2, which has a relatively high specific heat. Thus, in equal diffusion simulations, prior to autoignition not only must there be a decay of χ below χ_{crit}, but a larger amount of energy must be released (compared with no N_2 in the jet) before the mixture temperature increases to our definition of autoignition. On the other hand, when scalar gradients are high, the differential diffusion model allows the H_2 to diffuse rapidly away from the N_2 contained in the fuel stream, creating local mixtures with less N_2 which can ignite sooner.

Considering first large d for both diffusion models (and as seen with the pure H_2 fuel simulations), both τ_{ign} and ξ_{ign} asymptote respectively to $\tau_{hmi-ref}$ and to within the range of ξ_{MR}. For example, in burner environment 1 (1045 K coflow) at a pressure of 1 bar, as shown in Figure 3.4A, when d is greater than 10 mm, the autoignition delay time is equal

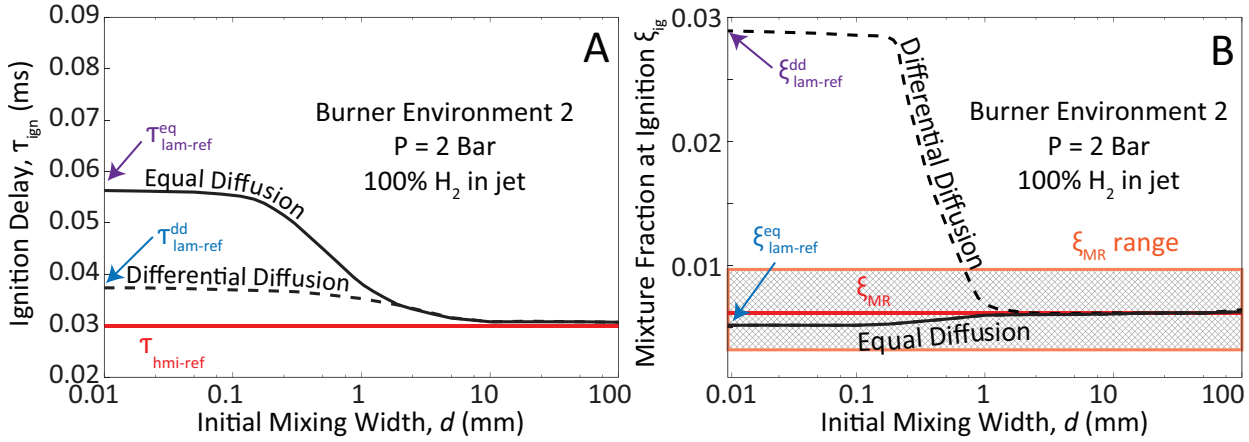

Figure 3.2: τ_{ig} vs. d (A) and ξ_{ig} vs d (B) for pure H_2 as the fuel in burner environment 2 at P = 2 bar for both equal and differential species diffusion models. For larger d, the species and temperature gradients are low and the mixture behaves as a homogeneous mixture, where τ_{ign} and ξ_{ign} are the same as the homogeneous values. However, at thin d, the high mass diffusivity of H_2 and time history of χ allow the differential diffusion model to ignite sooner than the equal diffusion model. Both models ignite later than the homogeneous model due to the high initial χ.

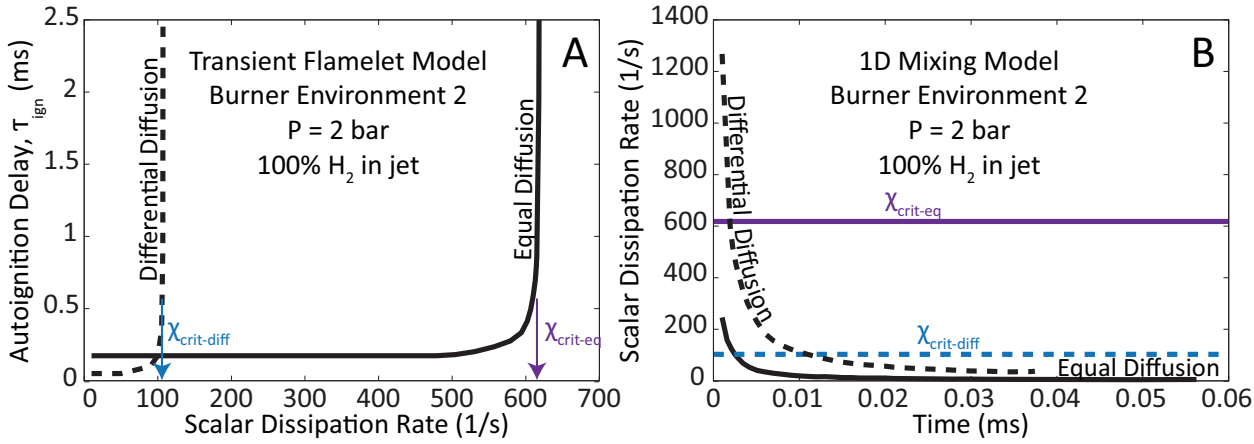

Figure 3.3: (A) plots τ_{ign} vs. χ for the mixture fraction at ignition ξ_{ign}, in burner environment 2 at 2 bar with 100% H_2 in the jet. The critical scalar dissipation rate χ_{crit} is defined where τ_{ign} increases exponentially. (B) plots the decay of χ for ξ_{ign}. The equal diffusivity simulation starts with χ below χ_{crit}, yet takes longer to ignite than the differential diffusion simulation due to the longer τign of the equal diffusion model. The initial mixing width is set to d = 0.1 mm.

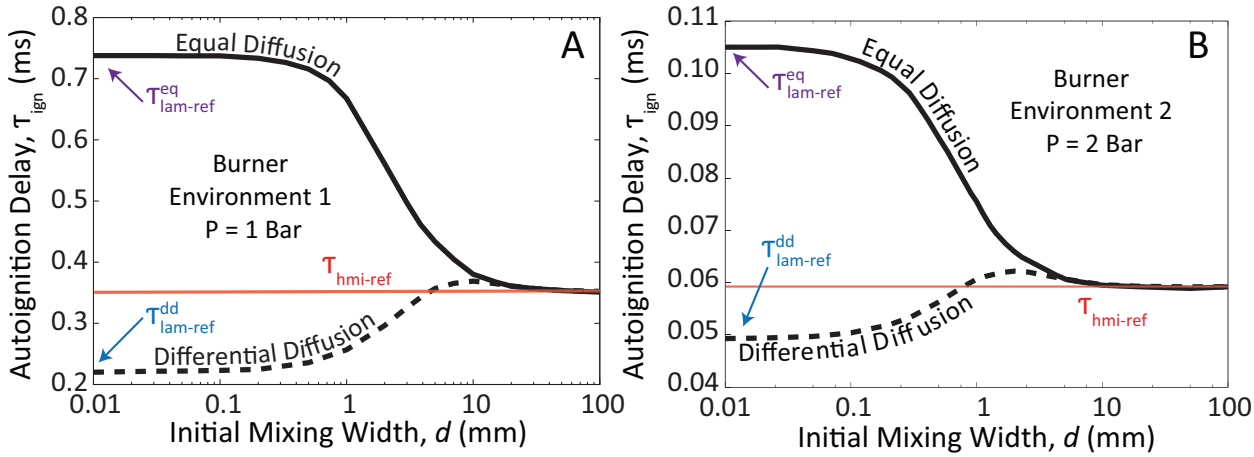

Figure 3.4: Autoignition delay time vs. Initial mixing width for (A) a 1045 K coflow at atmospheric pressure, (B) a 1200 K coflow at 2 bar for both equal and differential species diffusion models. The diffusion model used changes the autoignition delay for thin mixing widths, while for thick mixing width, both models asymptote to the HMI result.

to the predictions of the HMI calculations, i.e. 0.347 ms. Figure 3.4B shows a similar trend for burner environment 2 at a pressure of 2 bar, and additionally, the same trend is seen for all pressure considered (1, 2, & 5 bar). Furthermore, Figure 3.5 shows ξ_{ign} as a function of initial mixing width for both equal and differential diffusion models, where are large d, ξ_{ign} is in the range of ξ_{MR}.

At thin d, the effects of N_2 dilution become pronounced. For example, as shown in Figure 3.4A, at small mixing widths (less than $d = 0.1$ mm), an equal diffusion model predicts τ_{ign} = 0.738 ms, while a differential diffusion model predicts τ_{ign} = 0.220 ms. With N_2 in the fuel and for all conditions simulated, the differential diffusion model always ignites sooner than the equal diffusion model and additionally, the differential diffusion model predicts a τ_{ign} smaller than $\tau_{hmi-ref}$. The decrease observed in τ_{ign} for the differential diffusion model is due to the aforementioned ability of H_2 to leave the high heat capacity N_2 in the fuel behind. Additionally, as with the pure H_2 fuel results, in the differential diffusion model, the high mass diffusivity of H_2 relative to N_2 again leads to $\xi_{ign} > \xi_{MR}$, as seen in Figure 3.5. This is a result of: a) the water content in the oxidizer side (as is the case when the fuel is 100% H_2), and b) the differential diffusion mixture at ignition not being diluted by N_2 as is the case with equal diffusion. Figure 3.5 shows ξ_{ign} as a function of initial mixing

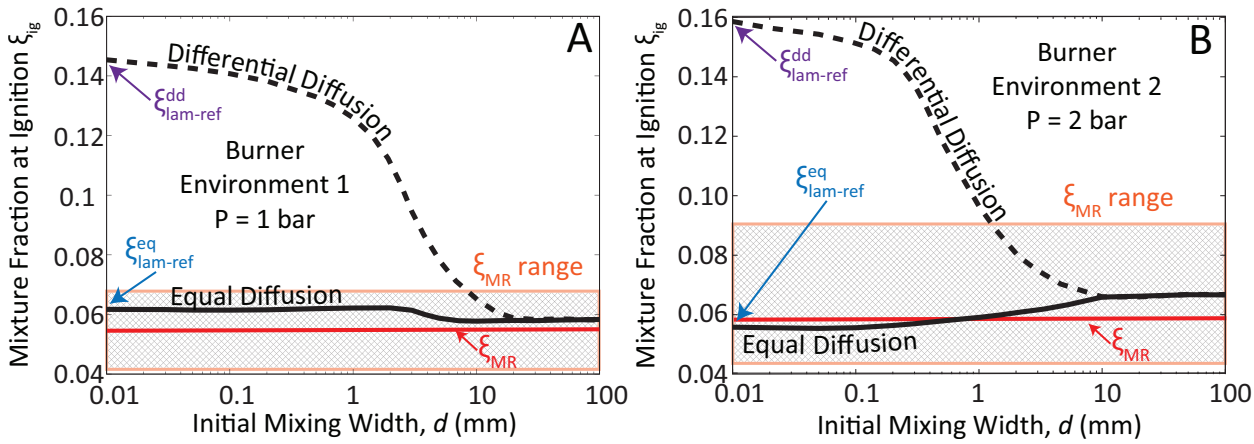

Figure 3.5: Plot A shows burner environment 1 (1045 K coflow)at atmospheric pressure, while plot B shows burner environment 2 (1200 K coflow) at 2 bar for both equal and differential species diffusion models. At thin mixing widths, the equal and differential diffusion ξ_{ig} asymptote to $\xi^{eq}_{lam-ref}$ and $\xi^{dd}_{lam-ref}$ respectively. As the mixing width increases, both models asymptote to near the HMI result. For thin mixing widths, the differential diffusion model ignites richer than the most reactive mixture fraction, ξ_{MR}.

width for both equal and differential diffusion models. Considering the differential diffusion model, as d increases, ξ_{ign} becomes leaner, and eventually asymptotes to the equal diffusion value. For all simulations (e.g. all pressures and coflow equivalence ratios), the same trend is seen where equal diffusion ignites around $\xi_{ign} \sim \xi_{MR}$ at all d. However, differential diffusion simulations ignite where $\xi_{ign} \geq \xi_{MR}$ for thin d and lean out to $\xi_{ign} \sim \xi_{MR}$ for wide d.

As previously mentioned, in the limit of small initial mixing widths we define a laminar reference mixture fraction at ignition and reference autoignition delay time based on diffusion model, (e.g. $\tau^{dd}_{lam-ref}$ and $\tau^{eq}_{lam-ref}$ where "dd" refers to differential diffusion and "eq" refers to equal diffusion). Additionally, $\xi^{eq}_{lam-ref}$ and $\xi^{dd}_{lam-ref}$ are defined (see Figure 3.5). Table 3.4 shows all reference values for HMI, equal diffusion, and differential diffusion models at 1, 2, and 5 bar and both burner environments (coflow temperatures of 1045 K and 1200 K). Comparing the laminar reference values with those predicted by HMI, it is seen that equal diffusion results (Le = 1) all fall near ξ_{MR} and are within the prescribed range of ξ_{MR}. However, compared to HMI and equal diffusion, differential diffusion simulations (non-unity Le) allow the mixture to ignite sooner and richer than equal diffusion simulations for thin d. Our results suggest that HMI calculations (as well as equal diffusion) cannot properly capture these trends due to the lack of proper accountability for transport effects.

The addition of N_2 to the fuel on the scalar dissipation rate needs consideration, as there is some coupling. As before, the transient flamelet model is used to obtain estimates χ_{crit}. Figure 3.6 shows the time evolution of scalar dissipation rate for burner environment 2 (1200 K coflow) at P = 2 bar and an initial mixing width of $d = 0.01$ mm. The scalar dissipation rate is tracked for the respective $\xi^{dd}_{lam-ref}$ and $\xi^{eq}_{lam-ref}$. As expected, initially χ is quite high, but decays exponentially as diffusion eases the species gradients. This same trend is seen for all cases where d is thin, as well as the case with 100% hydrogen as the fuel. Interestingly, τ_{ign} predicted by the flamelet model for both equal and differential diffusion is roughly the

	1 bar		2 bar		5 bar	
T_{coflow} [K]	1045	1200	1045	1200	1045	1200
$\tau_{hmi-ref}$ [ms]	0.347	0.088	9.51	0.058	19.9	0.297
$\tau^{eq}_{lam-ref}$ [ms]	0.740	0.151	28.3	0.105	62.9	0.848
$\tau^{dd}_{lam-ref}$ [ms]	0.200	0.074	0.867	0.043	11.9	0.080
$\xi_{hmi-ref}$	0.0544	0.0704	0.0347	0.0594	0.0347	0.0423
$\xi^{eq}_{lam-ref}$	0.0617	0.0603	0.0271	0.0558	input	0.0377
$\xi^{dd}_{lam-ref}$	0.1454	0.1594	0.1515	0.1586	0.1602	0.1674

Table 3.4: A comparison of reference values obtained from HMI and laminar LEM calculations. $\xi_{hmi-ref}$, $\xi^{eq}_{lam-ref}$, and $\xi^{dd}_{lam-ref}$ are the mixture fractions at ignition for the respective reference autoignition delay times. For all cases, differential diffusion ignites faster and richer than equal diffusion or HMI.

same, as seen in Figure 3.6A and unlike in the case with a fuel of pure H_2. However, the 1-D mixing model predicts autoignition sooner with the differential diffusion model, as seen in Figure 3.6B. These results seem to indicate that in laminar simulations with N_2 in the fuel, the relatively rapid decay of χ means its impact upon autoignition is lessened, and τ_{ign} is more greatly influenced by fuel N_2.

3.4.4 Comparison with Full Multicomponent Diffusion Model

As discussed in Section 2.4, a full multicomponent diffusion model including thermal diffusion was tested. The results (shown in Figure 3.7) suggest the simpler Lewis number formulation is adequate to capture the effects of differential diffusion. Very good agreement is seen between the full multicomponent model and the simpler Lewis number formulation, both in terms of τ_{ign} (Figure 3.7A) and ξ_{ign} (Figure 3.7B).

3.4.5 Comparison with Published Results

In an effort to validate the 1-D mixing model, simulations are compared to published results. *Knikker et al.* [2003] published results for a similar numerical domain, using both hydrogen and methane in their simulations. They too use SENKIN to find $\tau_{HMI-ref}$ and ξ_{MR}. For hydrogen, they use an oxidizer of heated air at a temperature of $T_{air} = 1100$ K, composed of 21% by volume of oxygen and 79% by volume of nitrogen (i.e. $X_{O_2} = 0.21$ and $X_{N_2} = 0.79$). Their fuel is hydrogen diluted in nitrogen at a temperature of $T_{fuel} = 300$ K, with a composition in mole fractions of $X_{H_2} = 0.25$ and $X_{N_2} = 0.75$. The stoichiometric mixture fraction for these conditions is $\xi_{st} = 0.56$. They run their simulation at atmospheric

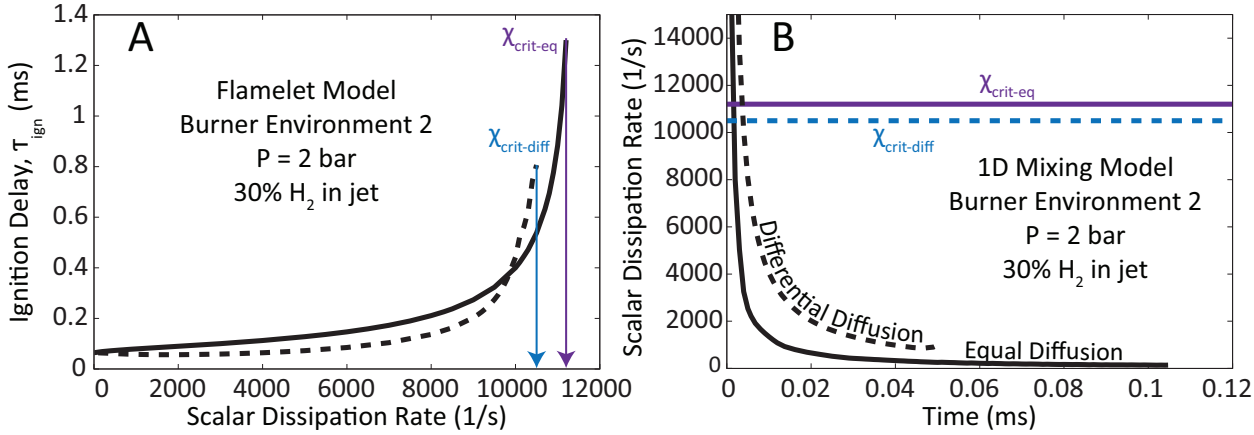

Figure 3.6: A time history of scalar dissipation rate at respective $\xi_{lam-ref}$ for Burner Environment 2, at P = 2 bar and an initial mixing width of d = 0.01 mm.

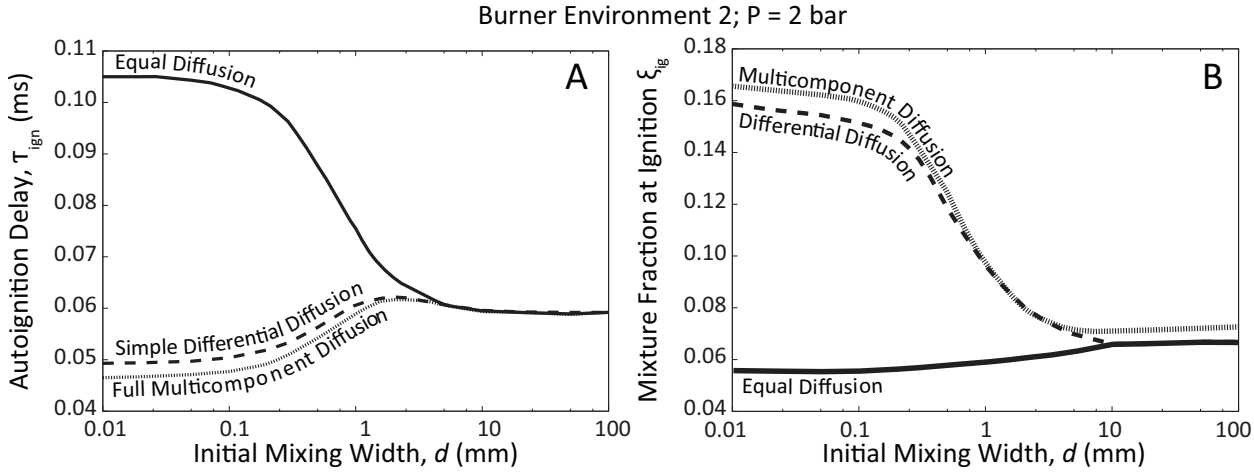

Figure 3.7: A comparison of the full multicomponent diffusion model with the simpler fixed Lewis number approach. Use of the simpler Lewis number formulation is warranted by the good agreement between the two models.

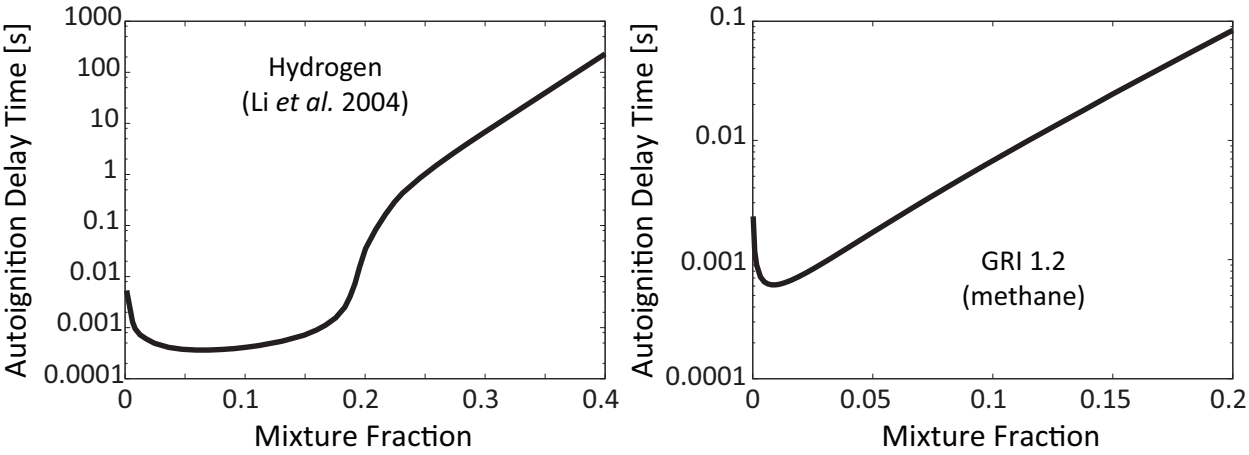

Figure 3.8: Results of HMI simulations with *Knikker et al.* [2003] parameters for both methane and hydrogen flames. Good agreement is seen in both cases.

pressure (1 atm), and use the kinetic mechanism of *Yetter et al.* [1991]. Note that some difference is expected as the Li *et al.* mechanism is used throughout the work presented in this dissertation. For methane, they used conditions chosen to give a minimum autoignition delay time around the same order of magnitude as the hydrogen simulation. Their oxidizer is again heated air, although the temperature is increased to $T_{air} = 1400$ K in order to reduce the autoignition delay time and thus the computational time required. Their fuel is a mix of methane and nitrogen, in equal volume fractions of $X_{CH_4} = 0.5$, $X_{N_2} = 0.5$, and at a temperature of $T_{fuel} = 300$ K. At these conditions, the stoichiometric mixture fraction is equal to $\xi_{st} = 0.14$. The pressure is 5 atm and a reduced (from GRI 1.2) 12-step methane mechanism by *Sung et al.* [1998] is used throughout, while simultaneously being validated against GRI 1.2, as well as GRI 3.0. For comparison in this dissertation, the full GRI 1.2 mechanism is used.

Knikker et al. [2003] use only the concept of ξ_{MR} but not a ξ_{MR} range, although they do comment on the wide range of reactive mixtures for hydrogen. For hydrogen, they find $\tau_{HMI-ref} = 0.34$ ms at $\xi_{MR} = 0.059$, in agreement with the results presented in Figure 3.8. For methane, autoignition as a function of mixture fraction tends towards the lean side, with no clear "most reactive" region. They find $\tau_{HMI-ref} = 0.49$ ms (again in agreement with Figure 3.8) and state the ξ_{MR} is not clearly definable as autoignition occurs on the extremely lean end of the mixture fraction range, and the temperature rise is not large enough (at 26 K) be described as "most reactive."

Knikker et al. [2003] additionally study the effect of the laminar initial mixing width on autoignition. Their method is similar to the results presented in this dissertation, although only differential diffusion models are used. Other differences exist: a) they use the definition of autoignition as described in 3.1 and 3.2, and b) they additionally investigate the effects of domain initialization. The results presented in section 3.4 assume equal diffusion in the creation of initial fuel/oxidizer profile. However, Knikker *et al.* show two results - one initialized using an equal diffusion assumption and the second using an initialization procedure imitating non-unity Lewis number effects. The initial species profiles are still described by an error function with an initial mixing width d, but the profile widths for

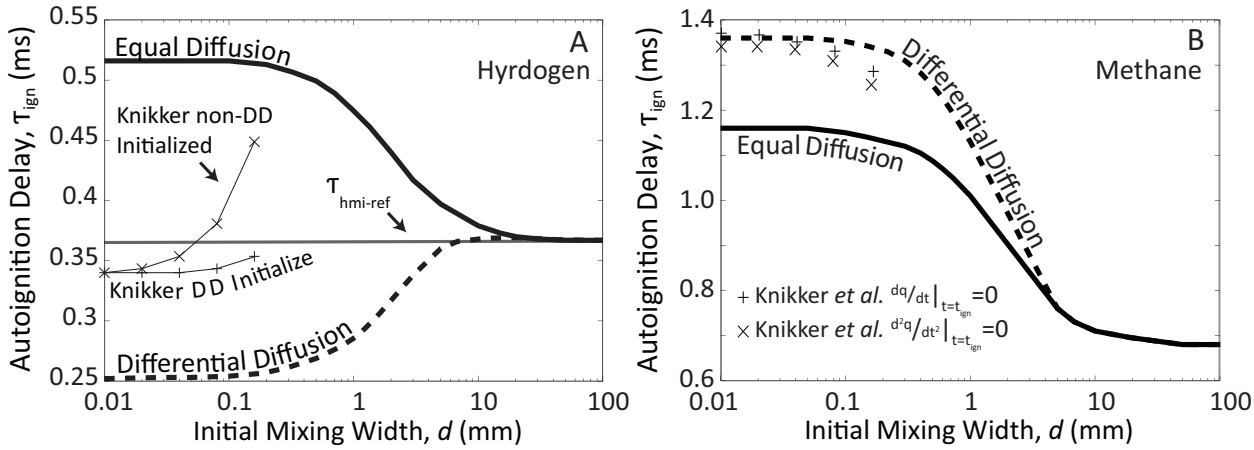

Figure 3.9: A comparison with *Knikker et al.* [2003] for both hydrogen (plot A) and methane (plot B) flames. Good agreement is seen for the methane flame, while the hydrogen flame shows a quite dissimilar trend.

the hydrogen and oxygen mass fraction, respectively, are now given by $d_{H_2} = \frac{d}{\sqrt{Le_{H_2}}}$ and $d_{O_2} = \frac{d}{\sqrt{Le_{O_2}}}$. The nitrogen mass fraction is calculated from the requirement that the sum of mass fractions must be equal to unity at each grid point. In their simulations, the hydrogen and oxygen Lewis numbers are set to $Le_{H_2} = 0.35$ and $Le_{H_2} = 1.2$, which corresponds roughly to the mean of the values found on the cold and hot sides, respectively. Thus, considering the differences in autoignition criteria and profile initialization, some difference in the comparison of the hydrogen results is expected.

Figure 3.9 presents results of the 1-D mixing models as well as the data of *Knikker et al.* [2003]. An interesting and opposite trend is observed for methane (Figure 3.9B), where the differential diffusion simulations autoignite slightly delayed compared to the equal diffusion simulations, although the magnitude of τ_{ign} is similar. The 1-D mixing model compares well with Knikker's result, and either definition of autoignition. However, the H_2 results are markedly different than Knikker's for hydrogen (shown in Figure 3.9A), although it is unclear why. One possibility is the difference in the initialization of the domain. *Knikker et al.* [2003] account for effects of differential diffusion in their initialization while we do not. For non-unity Lewis number initialization, Knikker predicts the hydrogen autoignition delay time as increasing with increasing d. The non-unity Lewis number initialization appears more sensitive to d than that of equal Lewis number initialization. Additionally, it appears that if d were to keep increasing, eventually autoignition would not occur for either initialization method, or would take an unreasonably long time to occur. However, it is also possible that if *Knikker et al.* [2003] had run simulation with larger initial mixing widths, their results may also have leveled out, as ours do, at large d. Alternatively, there is perhaps an error in Knikker's results, possibly due to under-resolution with increasing mixing width size, leading to inconsistent results. Wide d should produce a result similar to a homogeneously mixed condition.

3.5 Turbulent Mixing

For a turbulent mixing process, species transport is influenced by both molecular diffusion and/or turbulent stirring. Similar to the method adopted by *Sreedhara & Lakshmisha* [2002] and *Im et al.* [1998], two distinct regimes can be defined: $\tau_{turb} > \tau_{lam-ref}$ and $\tau_{turb} < \tau_{lam-ref}$, where τ_{turb} is the turbulence time scale and $\tau_{lam-ref}$ is based on the laminar thin mixing width result for respective diffusion models (either $\tau^{eq}_{lam-ref}$ or $\tau^{dd}_{lam-ref}$). For the $\tau_{turb} > \tau_{lam-ref}$ case, the turbulence time scale is fixed to at least $\tau_{turb} \sim 30\ \tau_{lam-ref}$, whereas for $\tau_{turb} < \tau_{lam-ref}$, the turbulence timescale is fixed to at most $\tau_{turb} \sim 0.3\ \tau_{lam-ref}$. If τ_{turb} is compared to $\tau_{hmi-ref}$ rather than $\tau_{lam-ref}$, in many cases a clear trend is not seen due to $\tau_{hmi-ref}$ being larger than $\tau^{dd}_{lam-ref}$ and smaller than $\tau^{eq}_{lam-ref}$.

Jet flames are simulated using the RANS PDF combustion model [*Chen & Kollmann*, 1989] for an estimate of the velocity fluctuation, u'. The jet flames are simulated over a range of pressures (1 bar < P < 5 bar) and Re_t (Re_t = 97, 297, 1000, 1500, 2000, 2500, 3000, & 4000). Simulations for $Re_t > 4000$ have proven too costly and such a high level of turbulence is rare in turbulent laboratory flames. Due to the stochastic nature of the LEM, at least five repeated simulations were performed for each Re_t considered, and the average value of τ_{ign} was taken. As the velocity fluctuation u' increases under enhanced turbulence, the integral length scale l_0 is adapted to keep τ_{turb} constant, where $\tau_{turb} = l_0/u'$, so thus $Re_t \propto l_0^2$. By use of this methodology, the influence of turbulent mixing is directly comparable for different turbulence parameters and consistent between simulations. The initial mixing width is chosen as $d = 0.1$ mm, which is roughly the minimum value observed where the laminar autoignition delay times no longer vary with decreasing mixing width (see Figures 3.4 and 3.5) and is also similar to the value used by *Im et al.* [1998] of $d = 0.09$ mm.

When $\tau_{turb} > \tau_{lam-ref}$, the time scale for turbulent mixing is much longer than the time scale for autoignition in the laminar case. It is therefore expected that turbulent mixing (parameterized by Re_t) would have little effect on species transport. Rather, the dominant and faster mixing process is due to molecular diffusion, as is the case in the laminar simulations. As shown in Figure 3.10, when Re_t increases, the autoignition delay time τ_{ign} is relatively constant and, in fact, similar to the value expected from $\tau_{lam-ref}$. As with the laminar results, computations with differential species diffusion always ignite faster than those with equal species diffusivity. Moreover, the mixture ignites at the laminar reference mixture fraction at ignition.

Figure 3.11 explicitly shows the similarity between the autoignition delay time and the reference timescales of $\tau_{hmi-ref}$ and $\tau_{lam-ref}$ when $\tau_{turb} > \tau_{lam-ref}$. In Figure 3.11A, τ_{ign} is normalized by $\tau_{hmi-ref}$, and no clear trend is observable, indicating the ineffectiveness of $\tau_{hmi-ref}$ as a reference timescale. However in Figure 3.11B, τ_{ign} is normalized by its respective $\tau_{lam-ref}$ (e.g. $\tau^{eq}_{lam-ref}$ or $\tau^{dd}_{lam-ref}$ for equal or differential diffusion models, respectively), where all results collapse to $\tau_{ign}/\tau_{lam-ref} \sim 1$. Thus, although $\tau_{hmi-ref}$ may be a quick way to calculate a reference autoignition delay time and most reactive mixture fraction, our results suggest that it is not the most appropriate one when differential diffusion is important, or even in the limit of sharp species gradients.

When $\tau_{turb} < \tau_{lam-ref}$, the time scale for turbulent mixing is much shorter than the autoignition time scale for a laminar diffusional process. In this case, it is expected that turbulent mixing (parameterized by Re_t) should have some influence on species transport,

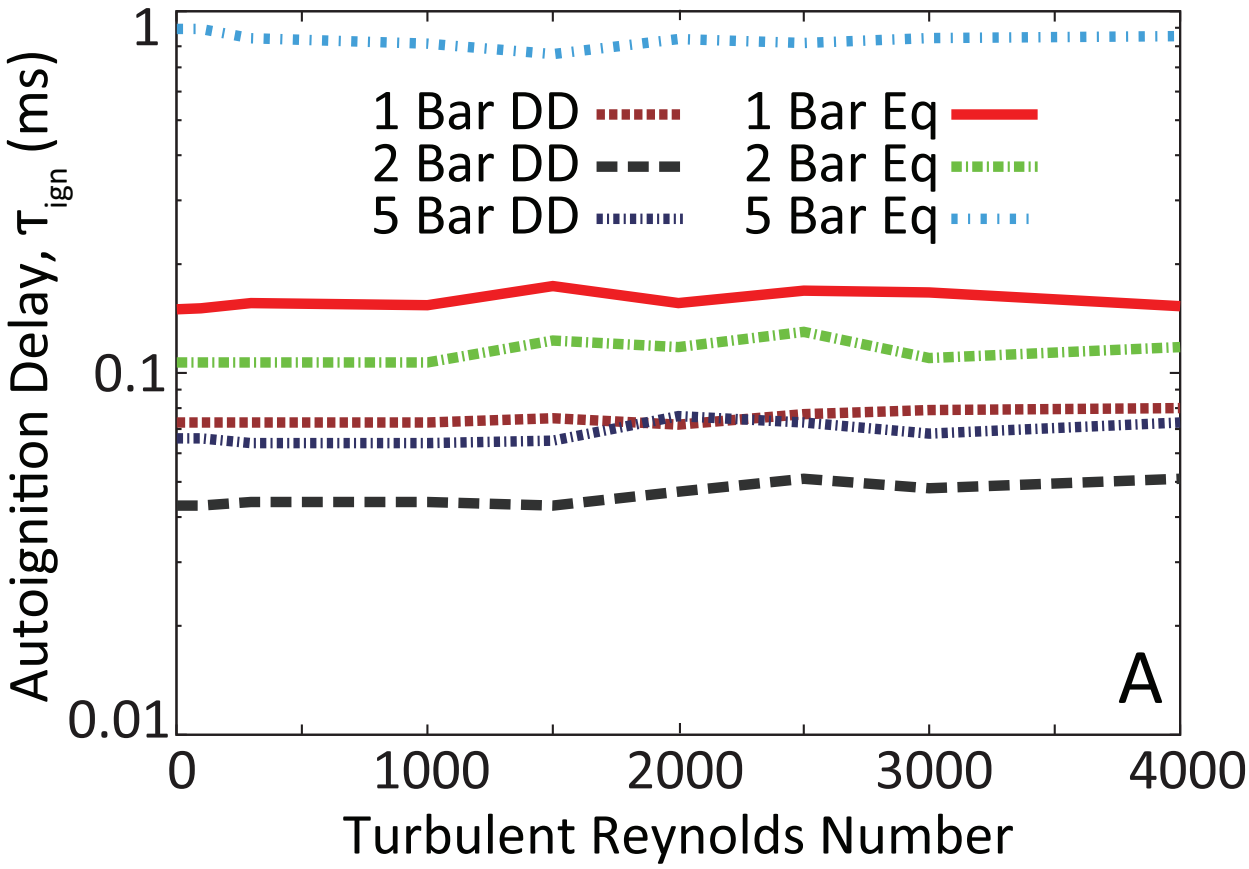

Figure 3.10: Autoignition delay time vs Re_t for all conditions simulated for Burner Environment 2 (1200 K coflow) when $\tau_{turb} > \tau_{lam-ref}$. Turbulence does not influence τ_{ign}. Note in the legend, "DD" refers to the differential diffusion model results, and "Eq" refers to the equal diffusion model results.

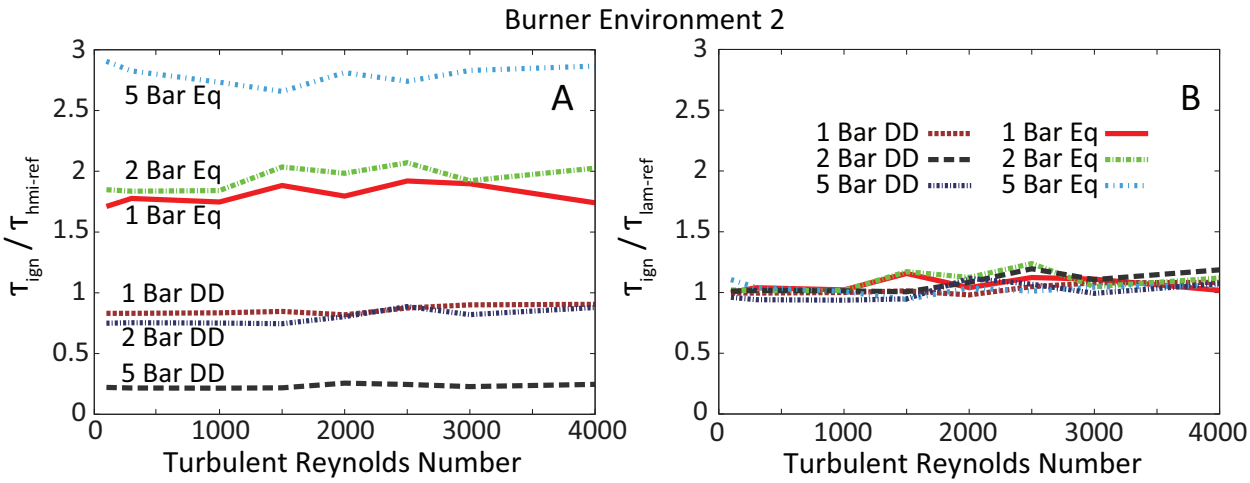

Figure 3.11: The same data presented in Figure 3.10, normalized in plot A by $\tau_{hmi-ref}$ and in plot B by $\tau_{lam-ref}$. Plot A shows no clear trend when normalized, while the normalization with $\tau_{lam-ref}$ (plot B) collapses the data to a single line, demonstrating the minimal effect of turbulence on autoignition delay when $\tau_{turb} > \tau_{lam-ref}$. Normalizing the above data by $\tau_{hmi-ref}$ shows no clear trend. Note the legend corresponds to both plots, where "DD" refers to the differential diffusion model results, and "Eq" refers to the equal diffusion model results.

as stirring enhances species mixing processes. However, when a differential species diffusion model is used, it is possible that hydrogen's high mobility due to molecular diffusion can compete with turbulent mixing and transport.

Two trends emerge which are dependent on the range of ξ_{MR}. For environments with a large range of ξ_{MR}, turbulence has a mild but noticeable impact, whereas for environments with a small range of ξ_{MR}, turbulence has a much greater impact. At pressures of 1 and 2 bar in burner environment 2, the range of most reactive mixture fraction is quite large, as compared with pressures in burner environment 1. Figure 3.12 shows τ_{ign} as a function of Re_t in burner environment 2 at pressures of 1 and 2 bar (where the range of ξMR is large). Figure 3.13 shows τ_{ign} as a function of Re_t in burner environment 1 at a pressure of 1 bar (where the range of ξ_{MR} is much smaller). All simulations show τ_{ign} at low Re_t occurs near the respective laminar reference values and that autoignition is delayed with increasing turbulence. However, the magnitude of delay is dependent on the range of ξ_{MR}.

We define the percent change in τ_{ign} as the difference between τ_{ign} at high Re_t and τ_{ign} at low Re_t, normalized by the shortest τ_{ign}. As the data is an average of several simulations, the trend is more important than the absolute values. In Figure 3.12, the change in τ_{ign} is roughly $\sim$ 10 to 50 % depending on diffusion model, with the differential diffusion model having a generally larger delay with increasing Re_t. In contrast, Figure 3.13 shows the effect of turbulence is much more dramatic. Here, τ_{ign} increases greatly with increasing Re_t, roughly $\sim$ 150 to 500 % depending on diffusion model, again with the differential diffusion model impacted more.

Our results compare well with the previous study by *Hilbert & Thévenin* [2002]. Figure 3.13 shows that Re_t has a minimal effect on τ_{ign} low Re_t ($Re_t = 97$, $Re_t = 297$) at atmospheric

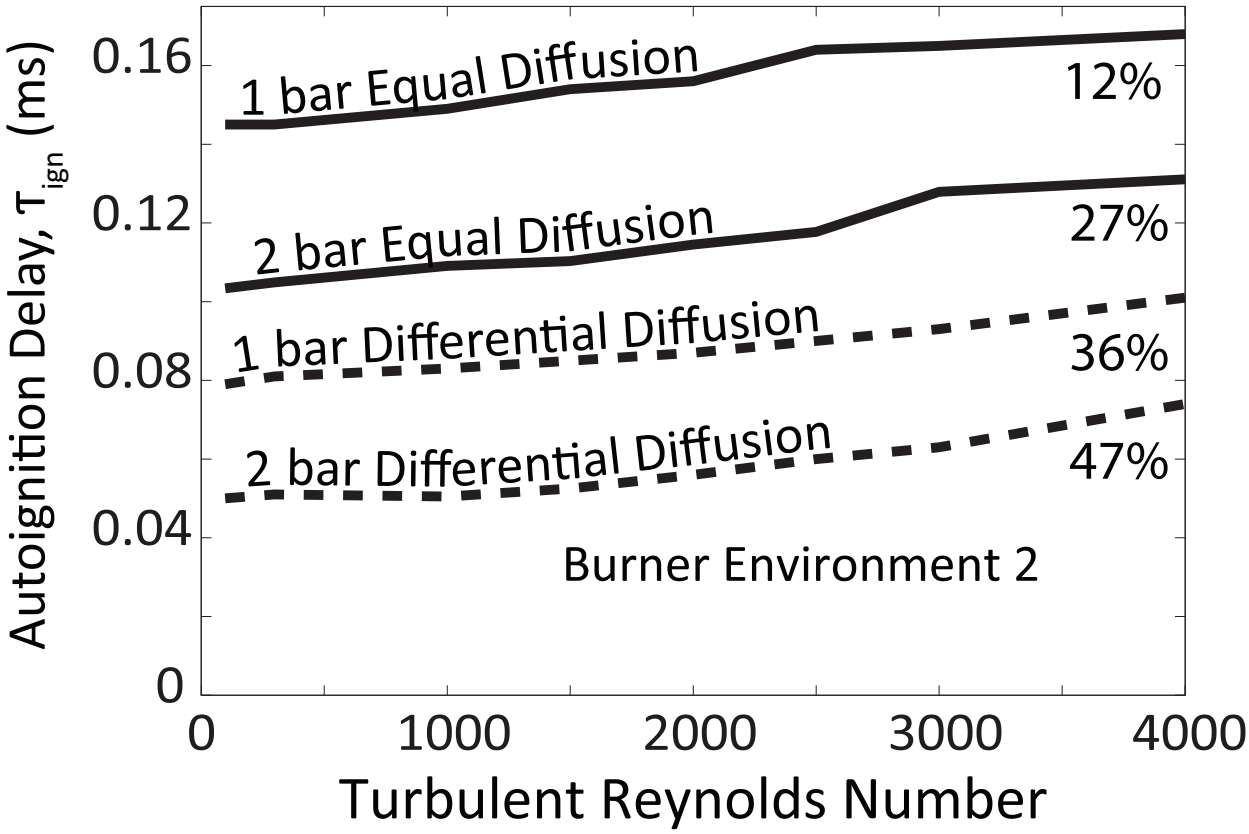

Figure 3.12: τ_{ign} versus Re_t. for pressures of 1 bar and 2 bar in burner environment 2 (1200 K coflow). A wide range of ξ_{MR} allows for turbulence to slightly impact τ_{ign}. In each simulation, t_{ign} starts near the laminar reference value (not shown for clarity purposes) and increases with Re_t.

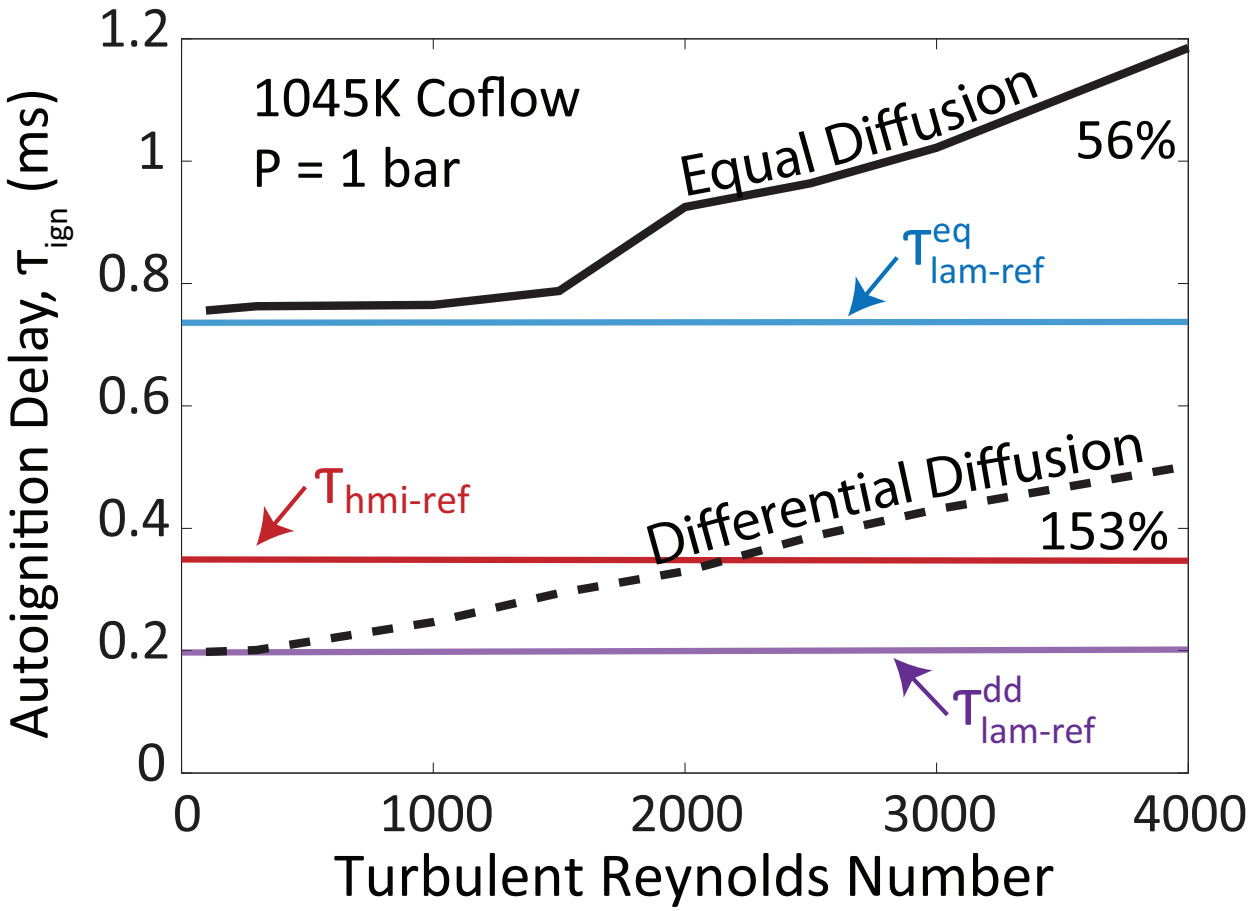

Figure 3.13: τ_{ign} versus Re_t. τ_{ign} as a function of Re_t for P = 1 bar in burner environment 1 (1045 K coflow). For these simulations, the range of ξ_{MR} is relatively small, and increasing turbulence significantly affects τ_{ign}. The percentage listed next to each diffusion model refers to the change in τ_{ign} from the lowest to highest Re_t.

pressure. The same results were presented by *Hilbert & Thévenin* [2002] with similar values of τ_{ign}. Indeed, at lower Re_t values, the effect of turbulence is minimal. However, as Re_t increases, the effect becomes much more pronounced and particularly in cases with a small range of ξ_{MR}.

The duality in the way turbulence affects autoignition delay time stems from the mixture fraction at ignition. Conditions where a wide range of ξ_{MR} exist allow many mixtures to begin autoigniting around the same time. Thus, although turbulent stirring may create regions of high scalar dissipation and delay autoignition in some region of the mixture fraction space, other regions are still able to autoignite and thus τ_{ign} is only slightly impacted. The opposite is true for mixtures with a small range of ξ_{MR}, where a mixing event might completely wipe out an autoigniting mixture fraction region, creating high scalar dissipation that must dissipate before autoignition can occur.

Figure 3.14 shows ξ_{ign} as a function of Re_t for burner environment 2 (1200 K coflow) at a pressure of 2 bar (a wide range of ξ_{MR}). Lines of best fit are set to the equal diffusion and differential diffusion models. Similar trends exist for the other conditions simulated

with a wide range of ξ_{MR} (namely, a pressure of 1 bar in burner environment 2). For low Re_t, the respective diffusion models autoignite near their laminar reference values. The equal diffusion model shows scatter in ξ_{ign} (shown with cross shapes on Figure 3.14) roughly within the range of ξ_{MR}. This indicates an increase in turbulence causes other reactive mixtures within the range ξ_{MR} to autoignite if the high scalar dissipation of a mixing event wipes out autoignition at or near $\xi^{eq}_{lam-ref}$. In the case of the differential diffusion model, as shown by the diamond shapes on Figure 3.14, increasing Re_t leads to very large scatter in ξ_{ign} at mixtures both richer and leaner than the range of ξ_{MR}. It is possible that the differential diffusion model allows for a wider range of reactive mixtures than the equal diffusion model. The wider possible range of reactive mixtures is indicated by the large range of scatter in the differential diffusion model. Increasing turbulence is able to mix out some of the autoigniting regions, but not all, as a large portion of the domain (or mixture fraction space) is reacting. The effect is a delay in τ_{ign} and the subsequently wide range of scatter in ξ_{ign}. Additionally, the differential diffusion model shows ξ_{ign} becomes leaner with increasing Re_t, and asymptotes to near the equal diffusion result.

For simulations with a narrow range of ξ_{MR}, the possibility of creating an autoignitable mixture at low scalar dissipation rate decreases as turbulence increases. Figure 3.13 shows ξ_{ign} as a function of Re_t for burner environment 1 (1045 K coflow) at a pressure of 1 bar (a narrow range of ξ_{MR}). Much less scatter is observed for both diffusion models, and lines connecting the average values of ξ_{ign} are plotted. As in simulations with a wide range of ξ_{MR}, the equal diffusion model ignites at mixtures within (or nearly within) the range of ξ_{MR}. However, unlike in simulations with a broad range of ξ_{MR}, the differential diffusion model always autoignites near $\xi^{dd}_{lam-ref}$, and does not asymptote to equal diffusion results.

In summary of the turbulent results, differential diffusion always autoignites sooner than equal diffusion, and generally richer. Both diffusion models capture effects of turbulence on τ_{ign}, however turbulence impacts the differential diffusion model slightly more than the equal diffusion model. For both τ_{ign} and ξ_{ign}, a homogeneous reference value does not accurately account for the effects of mixing and turbulence, and thus is an inadequate means of estimation. Mixtures with a large range of ξ_{MR} are less sensitive to turbulence than those with a small range of ξMR in terms of both τ_{ign} and ξ_{ign}. These results generally agree with previous studies by *Hilbert & Thévenin* [2002] and *Sreedhara & Lakshmisha* [2002], however several differences do exist in both results and methods. *Hilbert & Thévenin* [2002] used $\tau_{lam-ref}/\tau_{turb} = 0.5$ for all their 2-D DNS simulations, yet found turbulent simulations autoignited sooner than laminar ones. This is in contrast with this dissertation as well as *Sreedhara & Lakshmisha* [2002], who studied the effect of *decaying* homogeneous turbulence on a n-heptane / air mixture. Decaying turbulence indicates the turbulence timescale is constantly changing. They performed a number of simulations to account for τ_{turb} both longer and shorter than τ_{ref} and came to the same conclusion presented in this dissertation. Additionally, *Sreedhara & Lakshmisha* [2002] also found that autoignition occurs around ξ_{MR} and generally in the center of vortical structures where the scalar dissipation rate is lower. The implications of these results indicate the need for accurate representation of differential diffusion in engineering simulations such as RANS and Large Eddy Simulations. Often, combustion closure models in RANS and LES make assumptions about the mixedness in the subgrid - either well mixed or various models accounting for simple equal diffusion mixing. Additionally, many non-premixed combustion models assume combustion occurs at

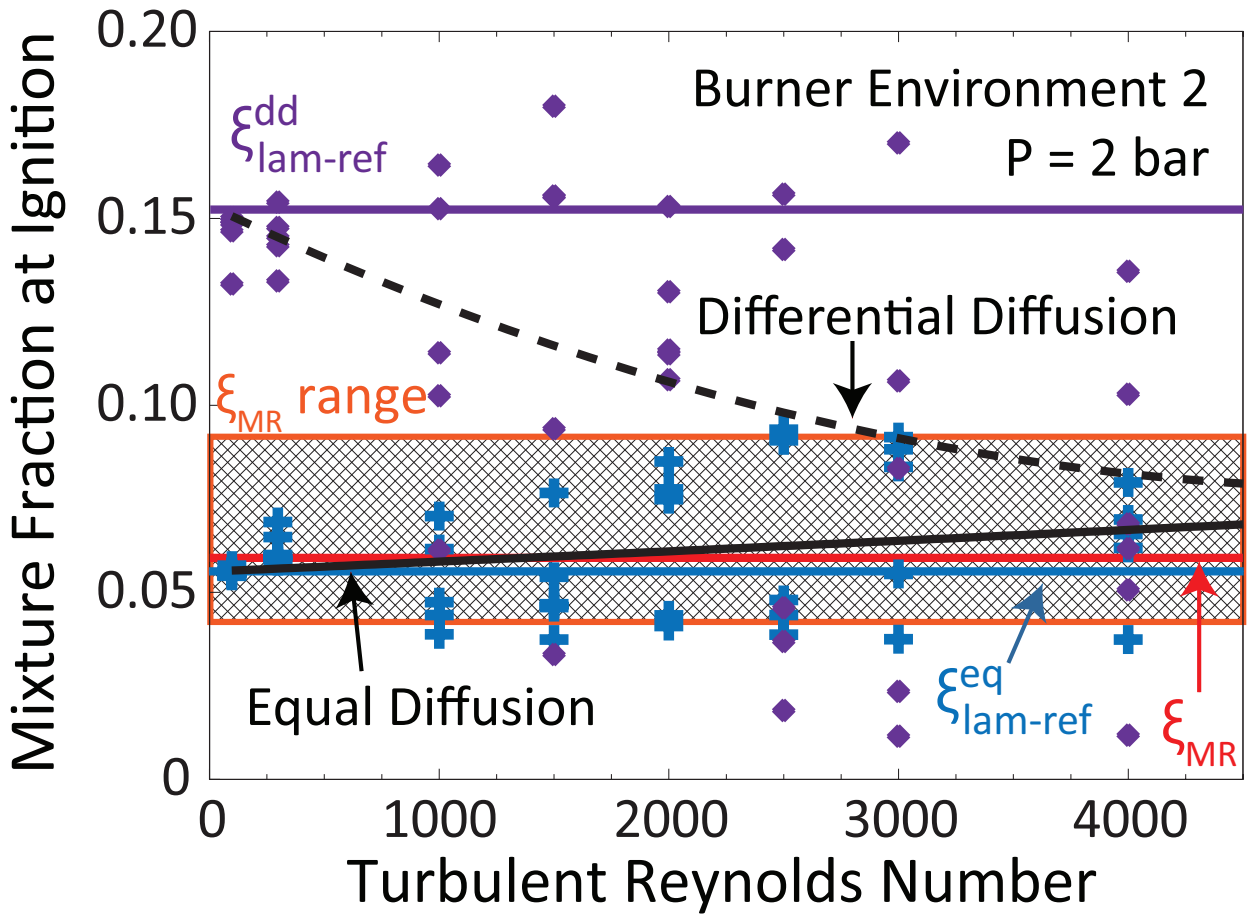

Figure 3.14: Mixture fraction at ignition (ξ_{ign}) for burner environment 2 (1200 K coflow) at a pressure of 2 bar (narrow range of ξ_{MR}). The average ξ_{ign} of the equal diffusion model stays near ξ_{MR} and $\xi^{eq}_{lam-ref}$ for all Re_t simulated. However, the average ξ_{ign} of the differential diffusion model autoignites near $\xi^{dd}_{lam-ref}$ at low Re_t and becomes leaner with increasing Re_t. The individual points of ξ_{ign} is indicated by diamonds for the differential diffusion model and crosses for equal diffusion.

a stoichiometric mixture fraction, contrary to the findings presented in this dissertation and in other works as mentioned above.

3.6 Conclusions

The autoignition of a H_2/N_2 jet flame in vitiated coflow is numerically investigated using a 1-D laminar mixing model and the 1-D Linear Eddy Model. Homogeneous mixture ignition calculations (via Senkin) are used as references in the 1-D models (i.e. $\tau_{hmi-ref}$ and a range of mixture fractions around ξ_{MR}). The computations with differential diffusion transport always autoignite sooner than the ones with equal diffusion transport. Moreover, for laminar autoignition delay time calculations, the initial mixing layer thickness is important as autoignition delay times and the mixture composition at ignition change greatly with the

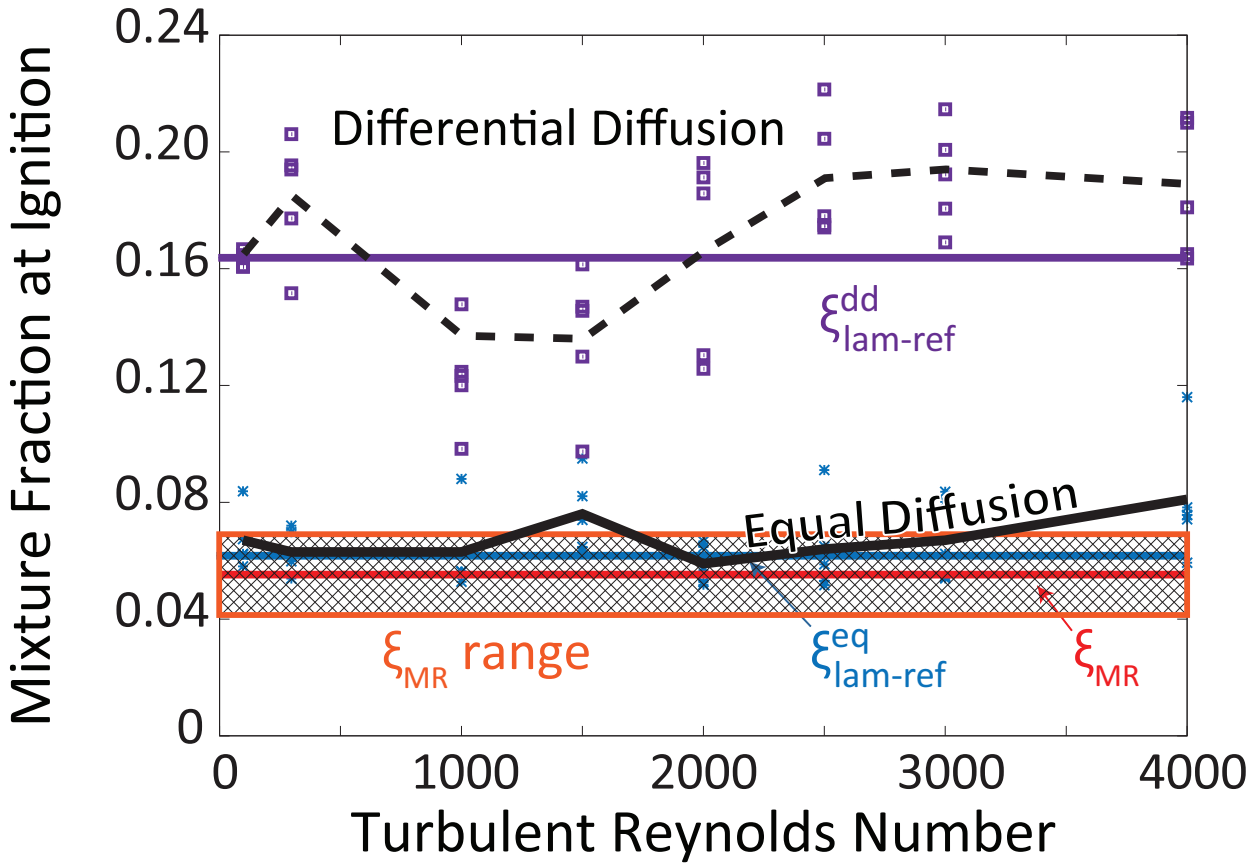

Figure 3.15: Mixture fraction at ignition (ξ_{ign}) for burner environment 1 (1045 K coflow) at a pressure of 1 bar. The average ξ_{ign} of the equal diffusion model stays near ξ_{MR} for all Re_t simulated. However, unlike simulations with a wide range of ξ_{MR}, ξ_{ign} of the differential diffusion model autoignites near $\xi^{dd}_{lam-ref}$ for all Re_t simulated. The scatter of ξ_{ign} is indicated by the boxes for differential diffusion and stars for equal diffusion.

diffusion model chosen. For an initial mixing width greater than roughly $d = 20$ mm, both models converge to $\tau_{hmi-ref}$ and roughly ξ_{MR}. However, because turbulent mixing creates sharp gradients, using $\tau_{hmi-ref}$ and ξ_{MR} as reference values may not be entirely appropriate. Computed results show that for small initial mixing widths (below roughly $d = 0.1$ mm), the laminar autoignition delay times are nearly constant, and differ significantly between diffusion models. Thus a unique autoignition delay reference time can be assigned for either the differential diffusion or equal diffusion model. Additionally, thin initial mixing widths autoignite at a mixture richer in differential diffusion simulations than in equal diffusion simulations, which is also often a separate composition than ξ_{MR}. In a differential diffusion model, the effect of N_2 dilution in the fuel leads to a decrease in τ_{ign} and a higher ξ_{ign} compared to a fuel of pure H_2. This is caused by the high penetration of light H_2 into the hot oxidizer where radical production is facilitated. Thus, although $\tau_{hmi-ref}$ and ξ_{MR} provide insight, they do not solely provide enough information as a reference for autoignition in hydrogen mixtures. However the range of ξ_{MR} does prove useful for turbulent simulations.

Turbulent LEM simulations are computed varying the turbulent Reynolds number as a parameter for turbulence intensity. The ratio τ_{turb} / τ_{ref} is kept constant at either $\sim$0.3 or $\sim$30, where τ_{ref} is a reference autoignition time. An important distinction over previous studies is to use τ_{ref} based upon the asymptotic limit of the 1-D laminar flame results for respective diffusion models. Doing so accounts for the mixing necessary to allow autoignition to occur, as opposed to using a homogenous reference. Two distinct regimes are defined, $\tau_{turb} > \tau_{ref}$ and $\tau_{turb} < \tau_{ref}$. When $\tau_{turb} > \tau_{ref}$, increasing Re_t has little impact on τ_{ign} or ξ_{ign} for either diffusion model. The turbulence timescale is simply too long, and τ_{ign} and ξ_{ign} correspond roughly to the respective diffusion model laminar reference values. When $\tau_{turb} < \tau_{ref}$, increasing Re_t delays autoignition from the laminar reference value, where the relative magnitude of the delay is dependent on the broadness of the range of ξ_{MR}. A large range of ξ_{MR} leads to a relatively small delay in τ_{ign} with increasing Re_t. Additionally, increasing Re_t in the differential diffusion model partially mutes the effects of differential diffusion on ξ_{ign} which asymptotes towards the equal diffusion / homogeneous value at high Re_t. A small range of ξ_{MR} allows a much greater delay in τ_{ign} and a much more constant ξ_{ign} with increasing Re_t. Importantly, for all turbulent computations using the equal diffusion model, ξ_{ign} deviates little from $\xi^{eq}_{lam-ref}$ and the range of ξ_{MR}. Thus, using an equal diffusion model does not capture the effects of turbulence on τ_{ign} or ξ_{ign}.

Chapter 4

Numerical Analysis of Experimentally Determined Stability Regions: Flame Propagation and Autoignition

4.1 Introduction

Anchoring of a hydrogen turbulent jet flame in a hot turbulent coflow is a problem of great theoretical and practical interest. The stabilizing anchoring mechanism of a lifted turbulent jet flame is thought to be controlled by either autoignition, flame propagation, or some combination of the two. The nature of flame stabilization was investigated experimentally by *North* [2013] using Berkeley's Vitiated Coflow Burner (VCB), shown in Figure 1.3 [*Cabra*, 2003]. The VCB consists of a high velocity fuel jet issuing into a coflowing stream containing products of lean premixed hydrogen combustion. The temperature of the coflow stream can be controlled by its stoichiometry. Nitrogen is added to the fuel jet to increase its momentum independent of jet velocity, which encourages the flame to lift from the nozzle. The goal of the current work is aimed at understanding the observed experimental trends by attempting to distinguish the anchoring mechanism of the lifted flames. Numerical simulations of the jet-in-coflow were performed to determine autoignition delay times of several fuel/oxidizer streams and to determine the local turbulent flame speed.

4.2 Experimental Methods, Background, and Results

Flame liftoff height is determined on Berkeley's VCB by measuring a time averaged ensemble of images obtained via schlieren imaging. The imaging setup is shown in Figure 4.1. A point light source is captured by the first spherical mirror, which sends a collimated beam of light across the burner. The light is reflected at the second spherical mirror, split with a knife edge at the focal point, and captured with a high speed camera. Figure 4.2 illustrates how liftoff height is determined from the schlieren image. A set of experiments were carried out at atmospheric pressure [*North*, 2013], with variations in (1) coflow equivalence ratios, ϕ_{coflow}, (and hence coflow temperatures) based on 100% H_2 and air ($0 < \phi_{coflow} < 0.35$), (2) the amount of N_2 content in the H_2 fuel jet ($0 < \%N_2 < 60$), and (3) the jet velocity, v_{jet} (v_{jet}

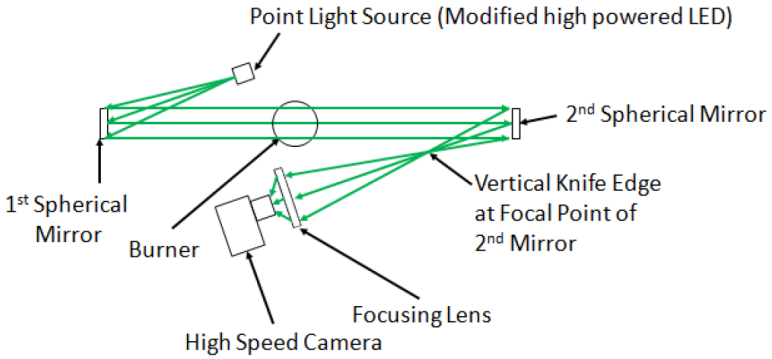

Figure 4.1: Experimental diagram used for Schlieren imaging to determine flame liftoff height.

= 300 m/s, 400 m/s, and 500 m/s). The coflow perforated plate diameter is 6 inches with a blockage of 89%. The central jet protrudes 1 inch above the perforated plate, with an outer diameter of 0.25 inches and an inner diameter of 0.093 inches.

Figure 4.3 presents anchoring stability maps for a turbulent jet flame from the experiments carried out by *North* [2013] for v_{jet} = 300 m/s and 500 m/s as a function of coflow equivalence ratio and the nitrogen content in the fuel. No data points are generated in the region between $0 < \phi_{coflow} < 0.15$ because the properties of the weak flame produced by the coflow were experimentally difficult to measure. Therefore, an assumed linear slope is shown until the first data point at $\phi_{coflow} = 0.15$. The autoignition temperature for hydrogen in quiescent air is roughly ~800K [*Patnaik*, 2007]. If the coflow is not hot enough to produce autoignition of the fuel jet (i.e. which corresponded to roughly ϕ_{coflow} 0.19), then the fuel jet required an external source of ignition, such as a lighter.

For a given coflow equivalence ratio, the amount of nitrogen in the hydrogen fuel jet is increased until the turbulent jet flame first lifts off. The coflow equivalence ratio and the nitrogen content in the fuel when the flame first lifts is marked by a square symbol in Figure 4.3. Increasing the nitrogen content further eventually leads to flame blowout, meaning the jet flame did not stay lit even when an external ignition source was provided. The coflow equivalence ratio and the nitrogen content in the fuel when the flame eventually blows out is marked by a triangle. The collection of liftoff (squares) and blowout (triangles) points at different coflow equivalence ratios are connected forming three regions. The region below the square boundary corresponds to conditions under which the jet flame is attached to the fuel nozzle. Under the conditions above the triangle boundary, the jet flame is blown out and does not stay lit even when an external ignition source is provided. In the region bounded by the square and the triangle boundaries, lifted turbulent jet flames are observed. As revealed in Figure 4.3, two distinct regions of the stability maps are identified, namely a lifted-steady flame region (i.e. anchored) and a lifted-unsteady flame region.

Given the stability diagrams, the goal of the following work is to dissect the observed experimental trends by distinguishing the stabilizing mechanism of the lifted jet flames. This is done with numerical simulations of the jet-in-coflow using the parabolic code to study both autoignition dominated regions as well as to investigate the plausibility of flame speed stabilization using the previously mentioned turbulent flame speed correlation post

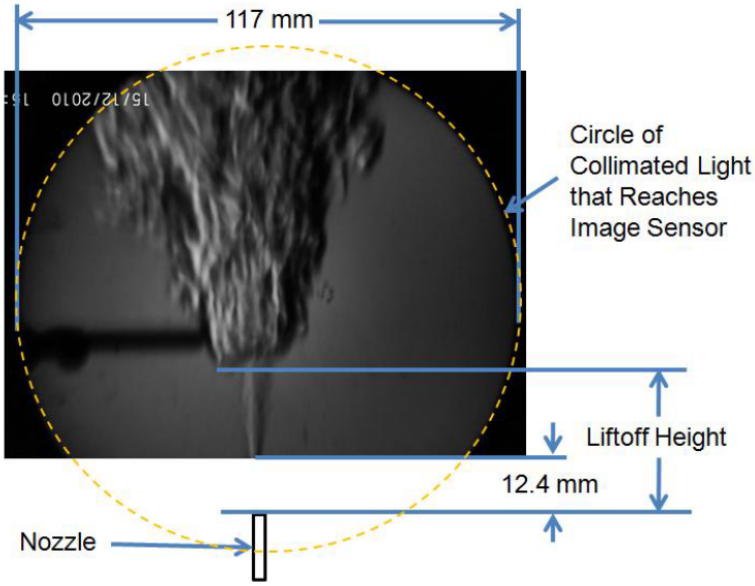

Figure 4.2: Sample high-speed image demonstrating how flame liftoff height is determined, from *North* [2013]

processing.

4.3 Numerical Methods and Results

4.3.1 Autoignition Delay Time

Because the fuel nitrogen content and coflow equivalence ratio are the two parameters used for characterizing the stability maps (see Figure 4.3), their influence on autoignition delay time and laminar flame speed is numerically investigated to establish their role in flame stabilization. The fuel jet mixes with the hot coflow stream, producing mixtures of various compositions and temperatures. With the equal chemical species diffusivity assumption, the mixture can be described by a conserved scalar, the mixture fraction, ξ. Values of $\xi = 1$ corresponds to pure fuel, while $\xi = 0$ corresponds to the oxidizer (coflow stream). The mixture with the minimal autoignition delay is often referred to as the most reactive mixture fraction ξ_{MR} [*Mastorakos*, 2009]. Because the coflow is very hot, autoignition will tend to occur near the coflow stream. As a result, the most reactive mixture fraction ξ_{MR} is often lean. For a given set of coflow stream and nitrogen content in the fuel jet, autoignition delay times are computed using Senkin [*Lutz et al.*, 1988] (0-D homogeneous) for a wide range of mixtures to identify ξ_{MR}. A detailed hydrogen-air mechanism by *Li et al.* [2004] is used. Coflow equivalence ratio is varied between $\phi_{coflow} = 0.2$ and $\phi_{coflow} = 0.25$, with N_2 fuel jet dilution ranging from 10% and 70%. The chemical state of the co-flow is determined by its equilibrium state.

The computed autoignition delay times versus mixture fraction are presented in Figure 4.4 for two coflow equivalence ratios: $\phi_{coflow} = 0.2$ on left and $\phi_{coflow} = 0.25$ on right. For cases when $\phi_{coflow} = 0.20$, increasing the N_2 content in the fuel jet from 10% to 50% broadens

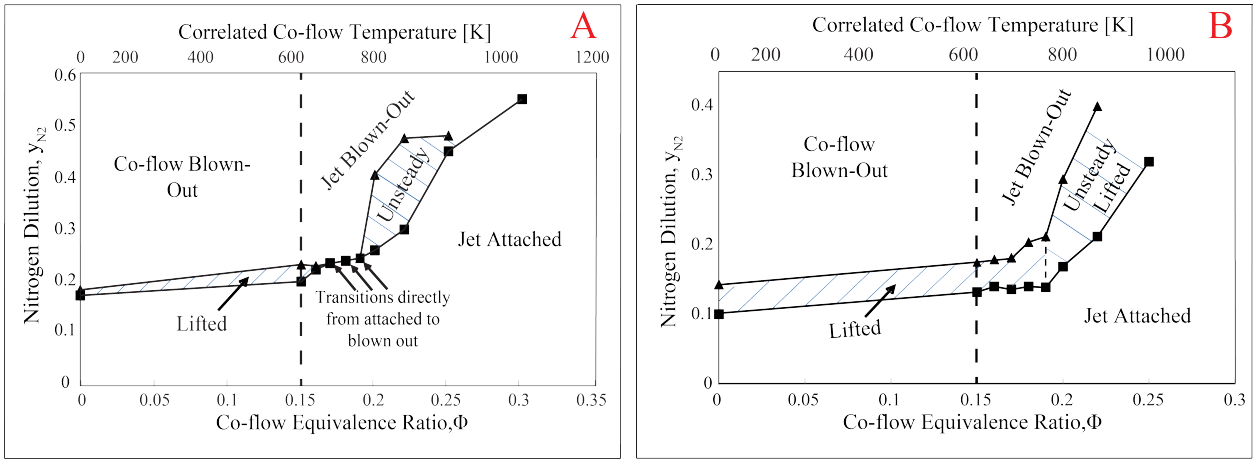

Figure 4.3: Stability regime diagram for $v_{jet} = 300$ m/s (A, left) and 500 m/s (B, right). At the slower jet velocity, when $\phi_{coflow} \sim 0.18$, the jet transitions from an attached flame to a blown out flame, with no lifted region. Increasing the jet velocity allows a lifted flame to develop for $\phi_{coflow} > 0.15$, while also creating a larger parameter space in which the flame is lifted. Source: [*North*, 2013]

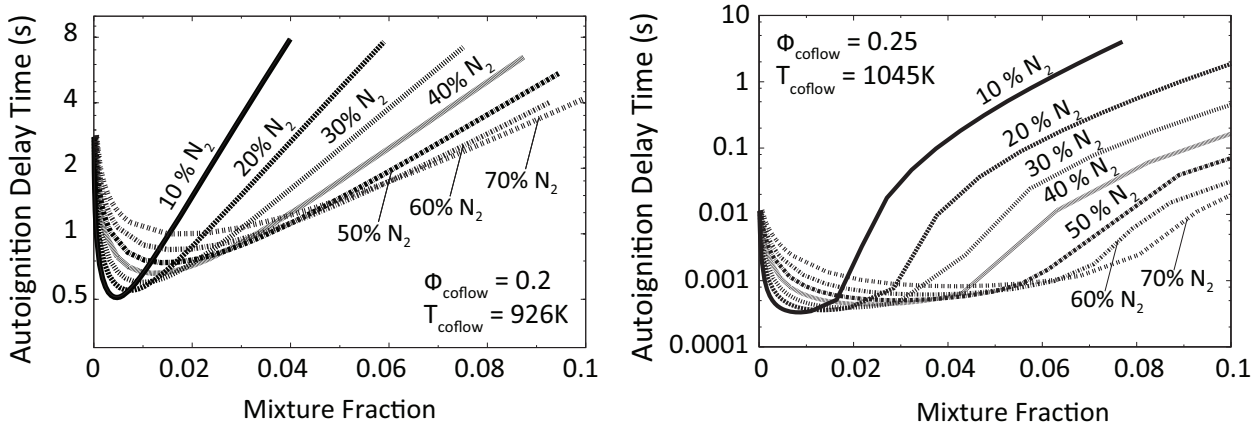

Figure 4.4: At lower ϕ_{coflow} ($\phi_{coflow} = 0.2$ on left), increasing the N_2 fuel jet dilution from 10% to 70% broadens the reactive mixture fractions. Increasing ϕ_{coflow} ($\phi_{coflow} = 0.25$ on right) creates a broad range of mixture fraction with a similar autoignition delay time.

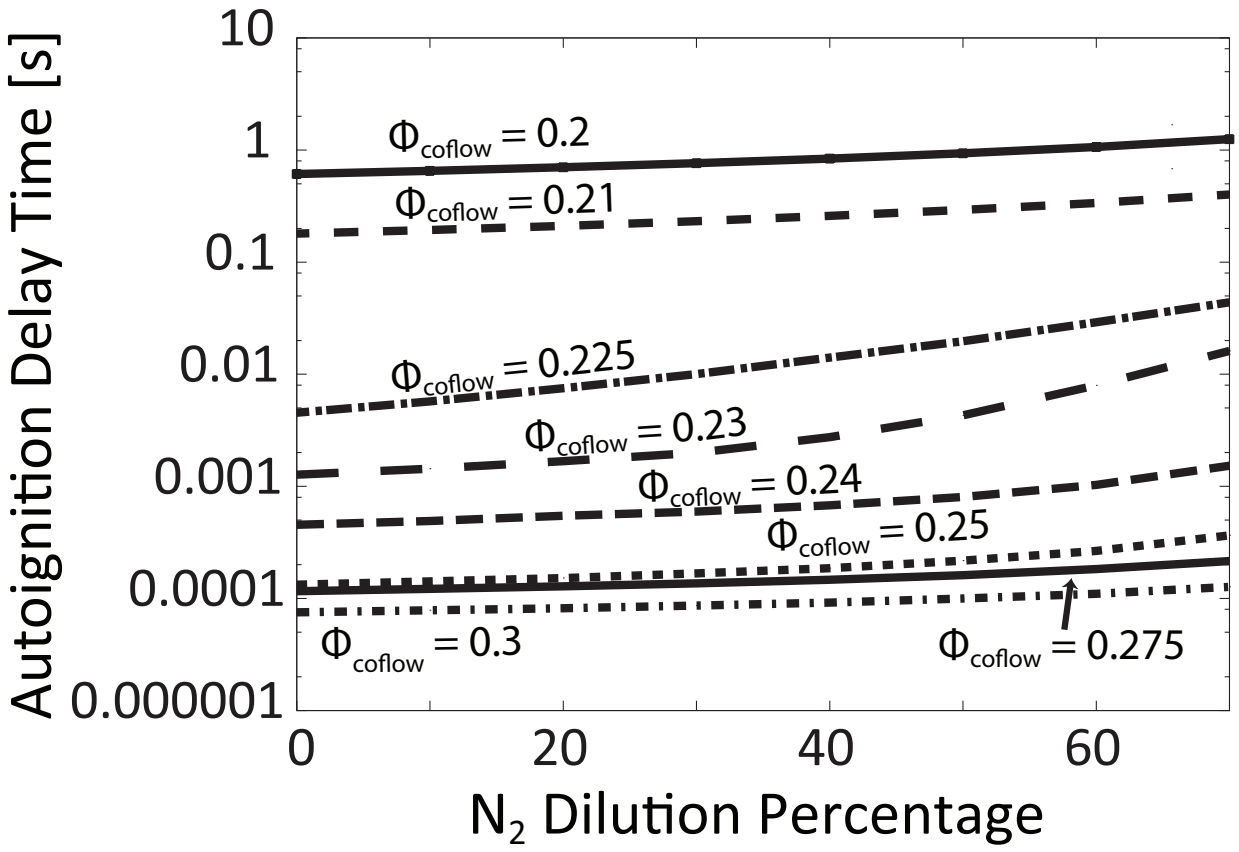

Figure 4.5: Minimum autoignition delay times vs N_2 dilution percentage. Increasing the coflow equivalence ratio decreases the effects of N_2 fuel jet dilution.

the most reactive mixture, but also slightly increases the minimum autoignition delay time. The corresponding results for $\phi_{coflow} = 0.25$ on the right of Figure 4.4 show a similar but more extreme trend. Similarly, increasing N_2 content broadens the range of most reactive mixtures for $\phi_{coflow} = 0.25$, however, variation in the N_2 content seems to have no significant effect on the minimum autoignition delay time. Comparing both cases, increasing ϕ_{coflow} generally creates a broader range of most reactive mixtures.

The minimum autoignition delay times are plotted versus N_2 content in Figure 4.5 for various coflow equivalence ratios. The results indicate the amount of N_2 dilution has a more significant effect on autoignition delay time at lower values of ϕ_{coflow}. For the highest coflow case $\phi_{coflow} = 0.3$, increasing N_2 content from 0% to 70% merely causes a $\sim$20% increase in the minimum autoignition delay time.

The dependence of minimum autoignition delay time on coflow equivalence ratio is shown in Figure 4.6. Between $\phi_{coflow} = 0.2$ and $\phi_{coflow} = 0.25$, the minimum delay times exhibit a very strong decreasing trend with coflow equivalence ratio or equivalently, coflow temperature. When the coflow temperature exceeds an upper limit, the decreasing trend becomes weaker. In short, the above computed results reveal that the minimum autoignition delay times decrease by almost four orders of magnitude when ϕ_{coflow} increases from 0.2 to 0.25. These results indicate that below $\phi_{coflow} = 0.25$, the impact of autoignition as a flame

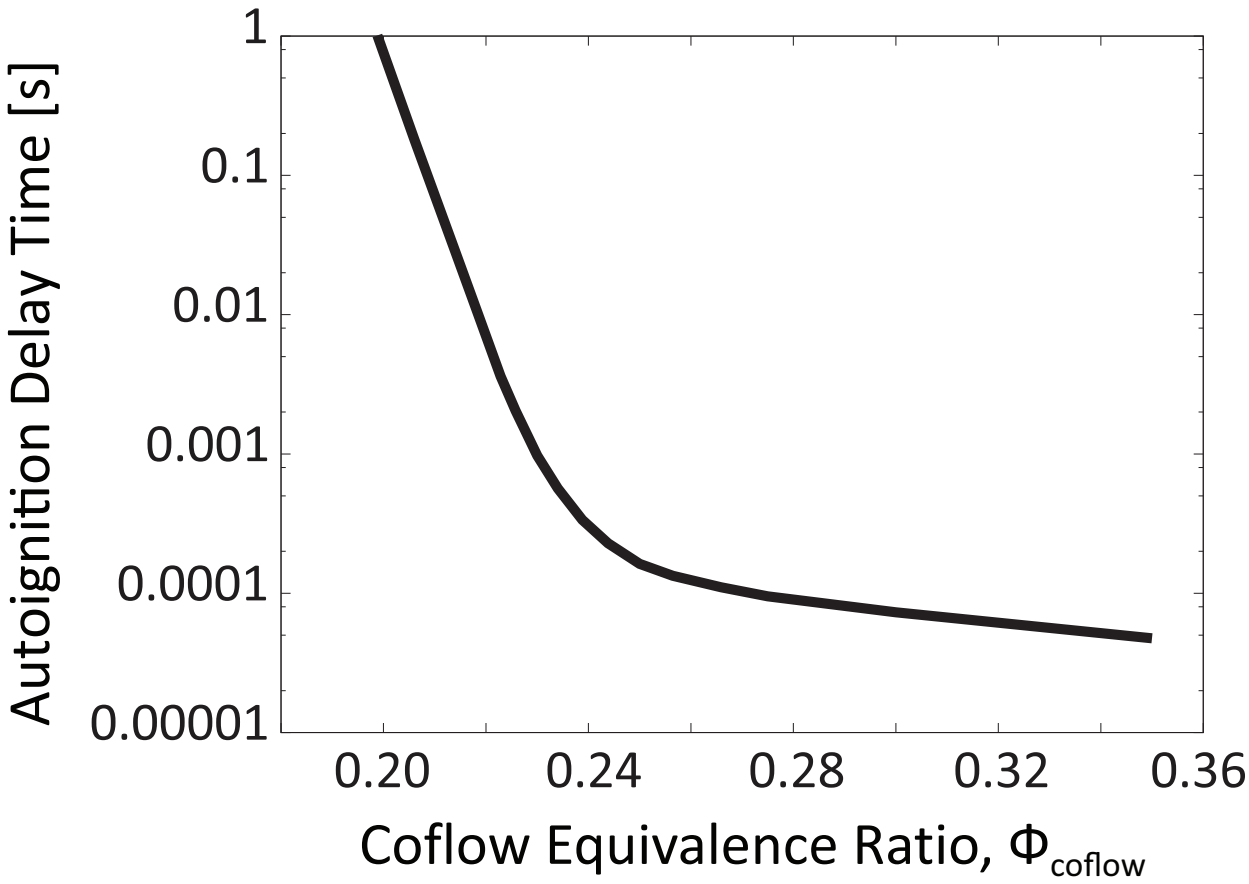

Figure 4.6: Minimum autoignition delay times vs coflow equivalence ratio, ϕ_{coflow}. For $\phi_{coflow} < 0.25$,the autoignition delay time shows a large sensitivity to ϕ_{coflow}, while above $\phi_{coflow} = 0.25$ the sensitivity is not as large.

stabilization mechanism is diminishing.

4.3.2 Flame Propagation

When $\phi_{coflow} < 0.20$, the coflow is simply too cold to allow for an autoignition flame, yet the experimental results show a flame is indeed possible. Hence, another flame stabilizing mechanism must be present. This other mode of stabilization is likely flame propagation based, and hence estimates of the flame speed for combinations of the jet and coflow are necessary. As discussed in Section 2.7, given coflow equivalence ratio and N_2 jet content, a global equivalence ratio is calculated and computed laminar flame speeds are fit to the form,

$$S_L(\phi_{global}) = \alpha \phi_{global}^{b} e^{(-c(\phi_{global}-d)} \tag{4.1}$$

where S_L is the laminar flame speed, and the coefficients a, b, c, and d are functions of N_2 fuel dilution (an example fit is shown on the left of Figure 4.7). The overall mixture equivalence ratio, ϕ_{global}, is based on fuel and coflow stream compositions, and is a function of radial and downstream position.

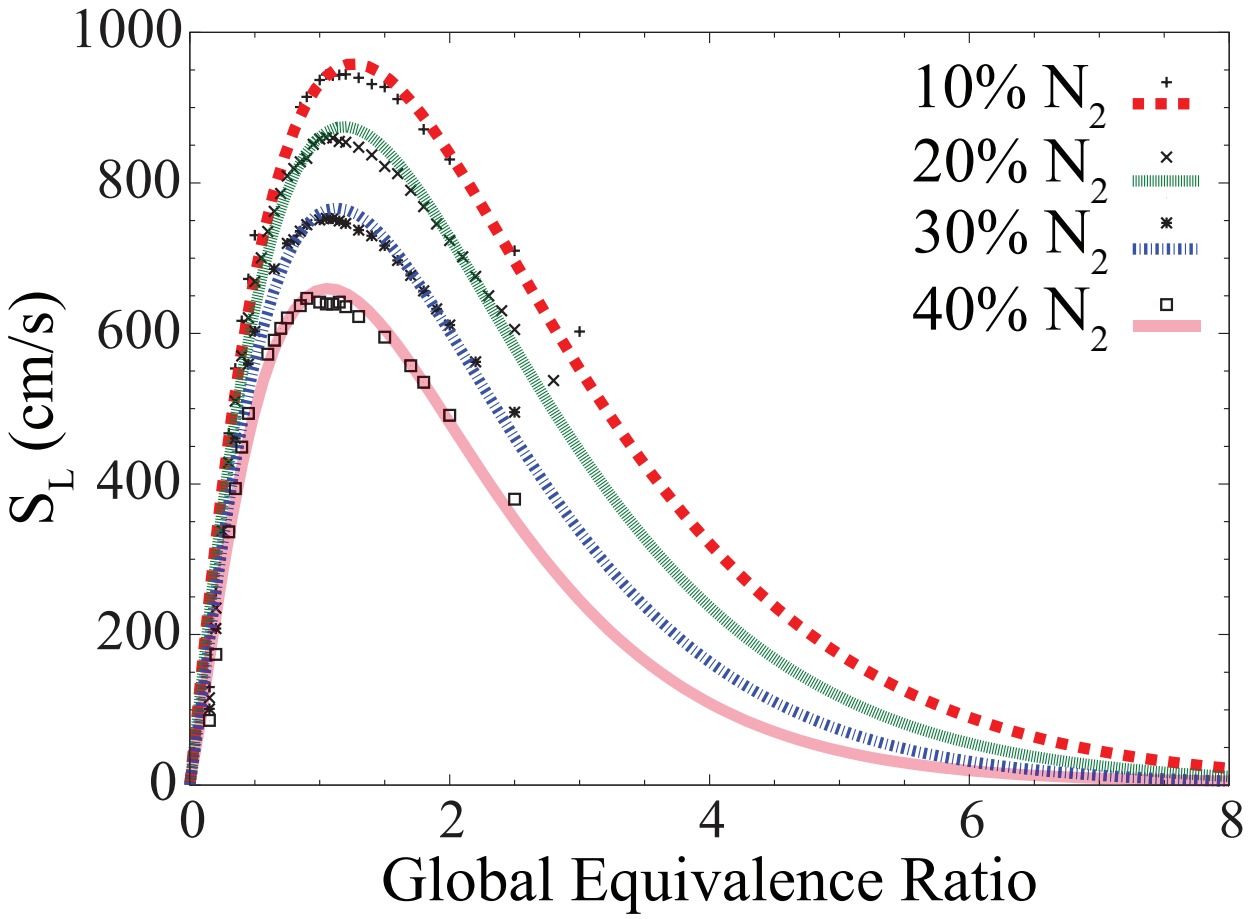

Figure 4.7: Computed results for the maximum laminar flame speed as a function of the global equivalence ratio and N_2 fuel dilution. An increase in fuel N_2 decreases flame speeds.

Figure 4.7 shows computed results for the maximum laminar flame speed as a function of the global equivalence ratio and N_2 fuel dilution. The maximum flame speed decreases with increasing N_2 dilution, and peaks near the stoichiometric global equivalence ratio. Additionally, the flame speed increases rapidly from lean global equivalent ratios to roughly stoichiometric, but decreases much slower for rich global equivalent ratios.

Analyzing the mechanisms of stability in lifted turbulent hydrogen jet flames is done using the parabolic code. The flow field is simulated as well as autoignition (if the coflow temperature allows) as detailed in Section 2.6. With additional novel post-processing (discussed in Section 2.7), regions within the jet and surrounding coflow are identified where a stable or anchored flame might exist. This is accomplished by comparing the local turbulent flame speed (S_T) to the local turbulent mean axial velocity ($\bar{U}$). Thus maps of regions where S_T is greater than the flow speed are created, indicating where a flame could exist via flame propagation. (see Figures 4.9 and 4.10). These maps can provide rough estimates of lift-off height and more importantly, the trend of flame stability behavior. One caveat to the post-processing approach is that when predicting areas where $S_T > \bar{U}$ when flame exists, the density, and hence velocity, are incorrect. However, the goal of the simulations is to capture the trend, and thus the method adopted is acceptable.

4.3.3 Results

Figures 4.8, 4.9, 4.10, and 4.11 show the temperature field (indicated by the colored contours) overlaid by the boundary where $S_T > \bar{U}$ (indicated by the dotted outline) for several values of ϕ_{coflow} and v_{jet}. The N_2 dilution increases from left to right in each snapshot, and trends closely with the N_2 dilution of the corresponding experiments (see Figure 4.3). When $\phi_{coflow} < 0.225$, the temperature field indicates that autoignition is not fast enough to initiate a flame, for both jet velocities considered (i.e., the temperature remains below the autoignition temperature everywhere in the domain). However, in the region where $S_T > \bar{U}$, the flame speed is high enough for an anchored flame to exist, given an external autoignition source, thus the dominant flame stabilization mechanism is most likely flame propagation.

At both $\phi_{coflow} = 0.15$ and $\phi_{coflow} = 0.2$, low values of N_2 dilution create the largest area where $S_T > \bar{U}$, and this region extends and touches the jet nozzle. When the $S_T > \bar{U}$ touches the nozzle, the flame is expected to be anchored and attached. Increasing N_2 dilution increases the momentum of the jet and also slows down the turbulent flame speed, causing a decrease in the area where $S_T > \bar{U}$, thus lifting the flame. Once the region where $S_T > \bar{U}$ becomes very tiny or disappears, the flame will be unstable and will ultimately blow out. For the case when $\phi_{coflow} = 0.15$ and $v_{jet} = 300$ m/s (Figure 4.8), a flame is no longer stable when N_2 dilution is increased above 25%. For the case when $\phi_{coflow} = 0.15$ and $v_{jet} = 500$ m/s (Figure 4.9), a flame is no longer stable when N_2 dilution is increased above 20%. Although it seems more intuitive that a lower velocity jet should allow a lifted flame over a larger range of N_2 dilution, competing effects between flame speed and jet momentum dispersion allow the opposite to be true. In other words, the 500 m/s jet has a wider range of N_2 dilution where a lifted flame exists. Less nitrogen dilution is needed to initially lift the flame (were it to exist) when the fuel jet has more initial momentum. The flame speed simulations predicted here correctly capture the trend shown previously in Figure 4.3.

For the case when $\phi_{coflow} = 0.2$ and $v_{jet} = 500$ m/s (Figure 4.10), autoignition still does not occur, even though the temperature field is hotter. Similar trends are observed to the results presented at a lower ϕ_{coflow} value. The lower values of N_2 dilution create the largest area where $S_T > \bar{U}$, and this region extends and touches the jet nozzle. A flame is no longer stable when N_2 dilution is increased to 40%. Again, the flame simulations predicted here correctly capture the trend shown previously in Figure 4.3.

For the case simulated when $\phi_{coflow} = 0.225$, and $v_{jet} = 500$ m/s, the coflow temperature becomes hot enough to cause autoignition of the fuel jet. Figure 4.11 shows temperature contours which indicate an autoignition flame. Because both an autoignition and flame propagation region exist, there are likely competing effects between these two stabilization mechanisms, but autoignition is believed to be the dominant mechanism. For example, autoignition occurs inside a majority of the regions where $S_T > \bar{U}$, but also outside of it, increasing the area where an anchored flame might exist. Similar to Figures 4.8, 4.9 and 4.10, each snapshot in Figure 4.11 shows the flame behavior with increasing N_2 dilution. As N_2 dilution is increased, the flame goes from attached and stable, to unstable and nearly blown out as the $S_T > \bar{U}$ region begins to shrink, and the temperature field cools (i.e. the autoignitable region diminishes). Unsteady flame behavior at higher N_2 dilution, as shown in the experimental results in Figure 4.3, may be due to the thinning and retreat of both the regions from the nozzle. Similar trends are seen for cases with different values of v_{jet}.

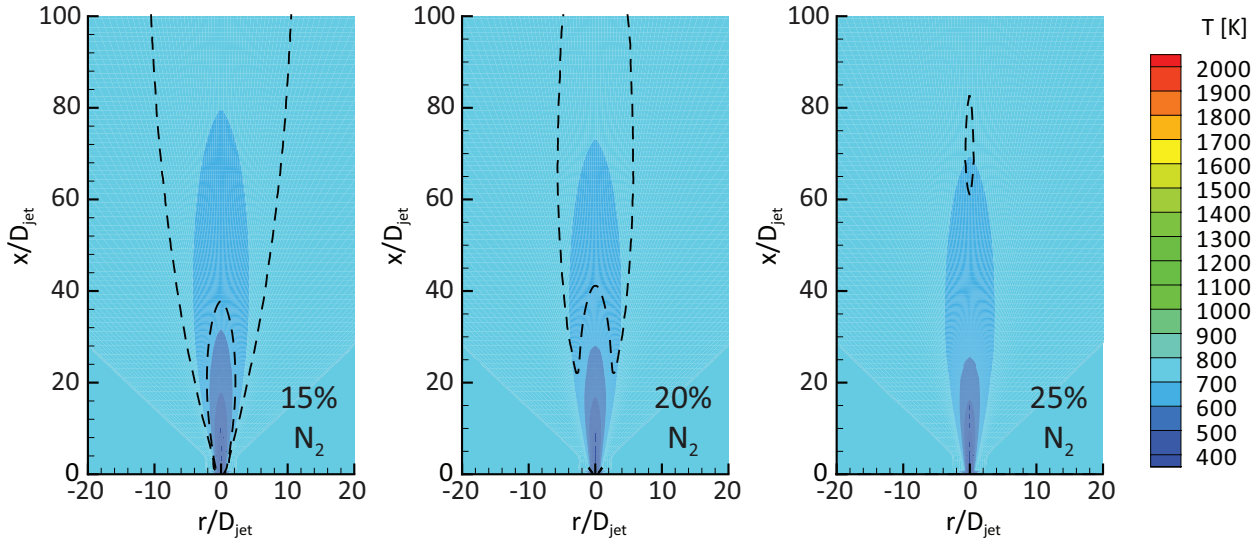

Figure 4.8: For $\phi_{coflow} = 0.15$, and a jet velocity of 300 m/s. Temperature contours indicate a temperature no higher than the coflow temperature and hence no flame exists. The dotted line indicates areas where $S_T > u'$. Increasing N_2 dilution causes a decrease in the area where $S_T > u'$, until the flame ultimately is not stable around 25% N_2 dilution. The trend (shown previously in Figure 4.3) is correctly captured.

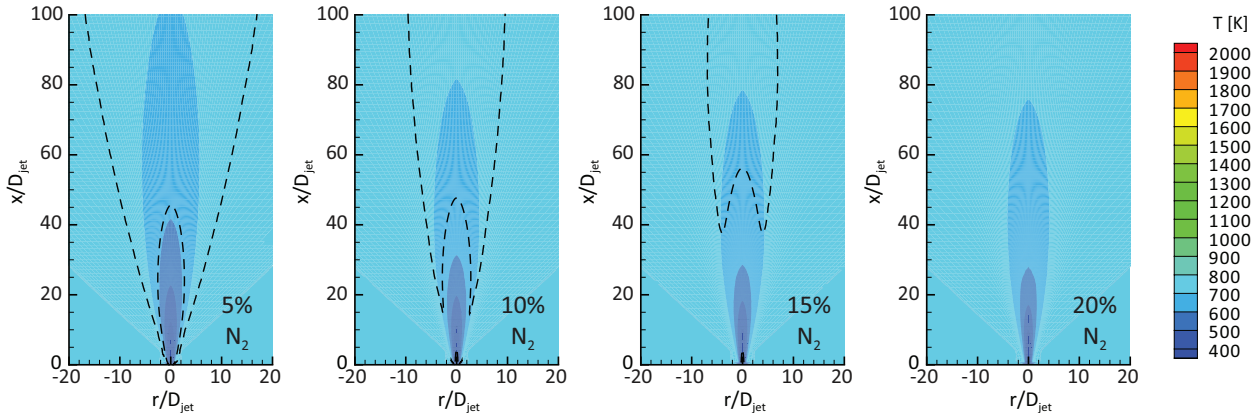

Figure 4.9: For $\phi_{coflow} = 0.15$, and a jet velocity of 500 m/s. Temperature contours indicate no flame. The dotted line indicates areas where $S_T > u'$. Increasing N_2 dilution causes a decrease in the area where $S_T > u'$, until the flame ultimately lifts, becomes unstable (diminished area) and then disappears. The trend (shown previously in Figure 4.3) is correctly captured.

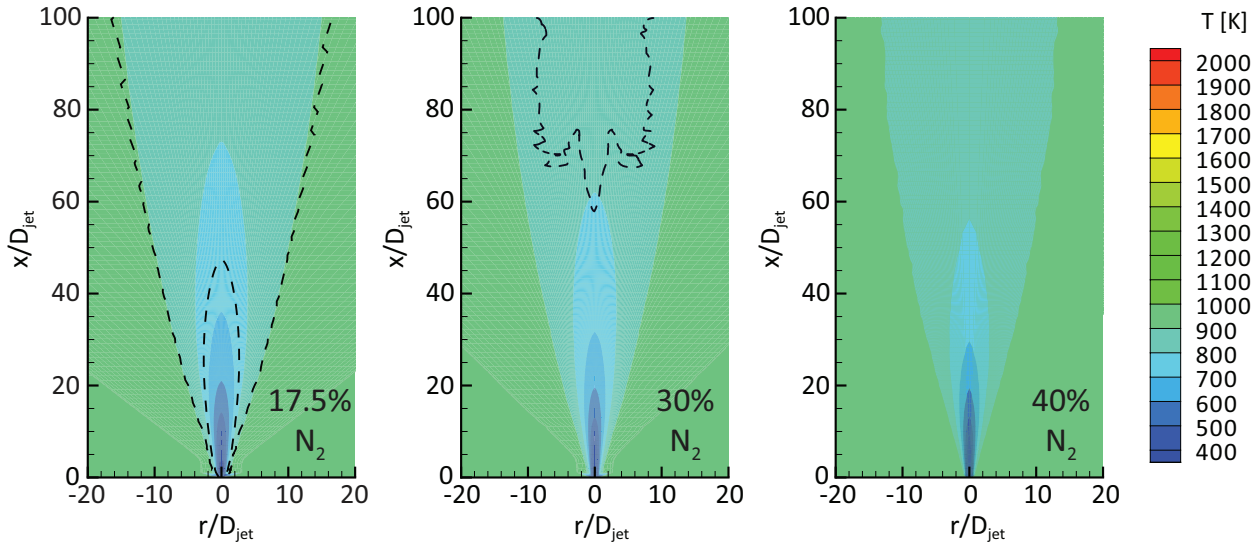

Figure 4.10: For $\phi_{coflow} = 0.2$, and a jet velocity of 500 m/s. Temperature contours indicate no flame. The dotted line indicates areas where $S_T > u'$. Again, increasing N_2 dilution from 17.5% (attached) to 40% (blown out) causes a decrease in the area where the flame stable.

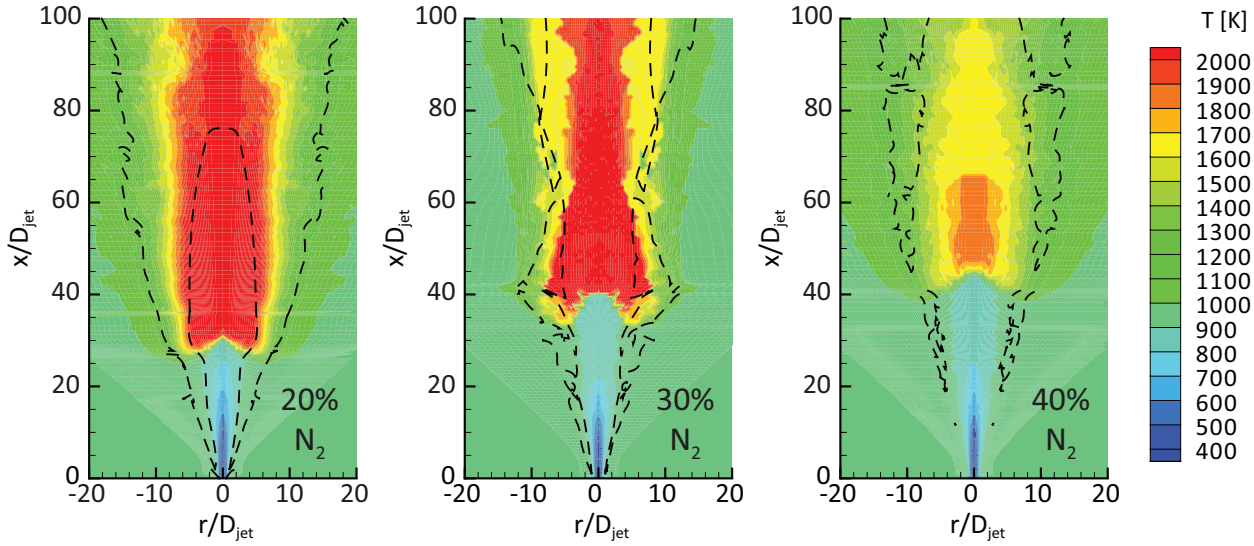

Figure 4.11: For $\phi_{coflow} = 0.225$, and a jet velocity of 500 m/s. Temperature contours indicate an autoignition flame, with regions where $S_T > u'$ are overlaid onto the temperature profile. Thus, an attached flame is shown at 0.2 N_2, and a nearly blown out flame is shown at 0.4 N_2, which agrees with experimental data.

4.4 Discussion and Conclusion

Two plausible flame stabilization mechanisms are considered for hydrogen turbulent jet flames in a vitiated coflow, namely autoignition and flame propagation. Novel model post-processing of results for attached, lifted, and lifted-unsteady regimes show that the correct trend is captured when compared to experimental results. Given the relative simplicity of the model concept, these results are encouraging and highlight the need for a multi-regime model (e.g. autoignition and flame propagation). At low coflow equivalence ratios, turbulent flame propagation is argued to be the main mechanism as the autoignition delay time is simply too long. At higher coflow equivalence ratios, autoignition is the main mechanism as the minimum autoignition delay time decreases by several orders of magnitude. Additionally, the model was useful to explain the discrepancy in the size of the lifted flame region when flame propagation dominates for different jet velocities and N_2 dilutions. Increasing the N_2 content in fuel increases fuel jet momentum, but also slows down turbulent flame speed. As N_2 content in fuel increases, the local turbulent mean axial velocity ($\bar{U}$) eventually blows out the flame. This is an important consideration in the design of gas turbine combustion chambers. Further work considering the effects of pressure would be the logical next step, as the chemical kinetics of H_2 combustion are quite pressure dependent.

However, there are apparent limitations in using a post processed 1-D model to predict flame propagation stabilization. The most obvious is that the flame itself is not computed, only a region of the flow field where the flame speed is fast enough to overcome the axial mean velocity is found. Secondly, the computed turbulent flame speed relies on an assumption that laminar and turbulent flame speeds are related and can be correlated. Although this is a common assumption [*Warnatz et al.*, 2006], it glosses over the real physics by introducing constants which are curve fit to match data [*Muppala et al.*, 2007]. Nevertheless, one possible enhancement to the model is to calculate S_T during the solution (instead of during post processing) and to then impose a burned solution and then recompute the flow field, accounting for the increased temperature, decreased density, and combustion products inherent in a flame. However, doing so would somewhat invalidate the simplicity of the model and additionally introduce unphysical flames (as it does not account for turbulence-chemistry interactions correctly). Part of the model's appeal is how quickly and inexpensively it can be used to provide guidance on experimentally observed trends. Thus, instead of further development of the post processing technique, future models should include the ability to account or both flame propagation and autoignition (i.e. a large scale RANS or LES). One promising possibility is an extension of the transient flamelet model (such as discussed in 2.5), called a Multidimensional Flamelet-generated Manifold, which is discussed in the following chapter.

Chapter 5

Concluding Remarks

The goal of this dissertation is derived from a desire to accurately predict lifted turbulent jet flames. The work is motivated by the problem of ever increasing energy needs coupled with a desire (and need) to reduce anthropogenic emissions. No single solution to this problem exists, but rather a portfolio of solutions across the board are needed. Carbon Capture and Storage is one promising option in that portfolio of new technologies becoming available in the quest to mitigate anthropogenic climate change. Due to its feasibility with current technologies, coupled with its possibilities still under research, such as the burning of hydrogen in gas turbines created by pre-combustion separation processes, it is a technology not too far off on the horizon. The necessity to predict the behavior of a lifted jet flame in a gas turbine is paramount to the development of large scale deployable power plants. The work contained in this dissertation highlights some current gaps in knowledge and applications in the modeling of hydrogen jet flames. One of the largest gaps is the ability to predict accurately how chemical kinetics are impacted by turbulence coupled with realistic molecular diffusion, as well as clearly understanding what mode of flame stabilization exists. Thus, the goal of the dissertation is to numerically investigate the fundamental phenomena occurring between mixing, turbulence, and chemistry at atmospheric to moderate pressures, and to identify dominant flame stabilization mechanisms for lifted turbulent jet flames. For conditions where autoignition dominates, the impact of turbulence and diffusion model on autoignition is highlighted. Additionally, it is shown that when the coflowing stream is too cold to allow for autoignition, flame propagation is the flame stabilization mechanism.

The autoignition of conditions in a H_2/N_2 jet flame in vitiated coflow is numerically investigated using a 1-D laminar mixing model and the 1-D Linear Eddy Model. Homogeneous mixture ignition calculations (via Senkin) are used as references in the 1-D models (i.e. $\tau_{hmi-ref}$ and a range of mixture fractions around ξ_{MR}). Pressure increases impact all models in a similar manner, typically delaying autoignition. For laminar autoignition delay time calculations, the initial mixing layer thickness is important as autoignition delay times and the mixture composition at ignition change greatly with the diffusion model chosen. In all cases, the scalar dissipation rate must decay sufficiently to allow for autoignition to occur. Additionally, turbulent mixing creates sharp gradients, and thus using $\tau_{hmi-ref}$ and ξ_{MR} as reference values may not be entirely appropriate. Computed results show that for small initial mixing widths (below roughly $d = 0.1$ mm), the laminar autoignition delay times are nearly constant, and differ significantly between diffusion models. Thus a unique

autoignition delay reference time is assigned for either the differential diffusion or equal diffusion model. Additionally, thin initial mixing widths autoignite at a mixture richer in differential diffusion simulations than in equal diffusion simulations, which is also often a separate composition than ξ_{MR}. In a differential diffusion model, the effect of N_2 dilution in the fuel leads to a decrease in τ_{ign} and a higher ξ_{ign} compared to a fuel of pure H_2. This is caused by the high penetration of light H_2 into the hot oxidizer where radical production is facilitated. Thus, although $\tau_{hmi-ref}$ and ξ_{MR} provide insight, they do not solely provide enough information as a reference for autoignition in hydrogen mixtures. However the range of ξ_{MR} does prove useful for turbulent simulations.

Turbulent LEM simulations further highlight the importance of diffusion model choice and are computed varying the turbulent Reynolds number as a parameter for turbulence intensity. The ratio τ_{turb} / τ_{ref} is kept constant at either $\sim$0.3 or $\sim$30, where τ_{ref} is a reference autoignition time. An important distinction over previous studies is to use τ_{ref} based upon the asymptotic thin d limit of the 1-D laminar flame results for respective diffusion models. Two distinct regimes are defined, $\tau_{turb} > \tau_{ref}$ and $\tau_{turb} < \tau_{ref}$. When $\tau_{turb} > \tau_{ref}$, increasing Re_t has little impact on τ_{ign} or ξ_{ign} for either diffusion model. The turbulence timescale is simply too long, and τ_{ign} and ξ_{ign} correspond roughly to the respective diffusion model laminar reference values. When $\tau_{turb} < \tau_{ref}$, increasing Re_t delays autoignition from the laminar reference value, where the relative magnitude of the delay is dependent on the broadness of the range of ξ_{MR}. A large range of ξ_{MR} leads to a relatively small delay in τ_{ign} with increasing Re_t. Additionally, increasing Re_t in the differential diffusion model partially mutes the effects of differential diffusion on ξ_{ign} which asymptotes towards the equal diffusion / homogeneous value at high Re_t. A small range of ξ_{MR} allows a much greater delay in τ_{ign} and a much less variable ξ_{ign} with increasing Re_t. Importantly, for all turbulent computations using the equal diffusion model, ξ_{ign} deviates little from $\xi^{eq}_{lam-ref}$ and the range of ξ_{MR}. Thus, using an equal diffusion model does not capture the effects of turbulence on τ_{ign} or ξ_{ign}. The computations with differential diffusion transport always autoignite sooner than the ones with equal diffusion transport, as well as richer (for thin mixing widths), important due to the widespread use of equal diffusion models, especially in RANS and LES models. An equal diffusion assumption in large scale models will predict autoignition too late and at an incorrect mixture, thus simulating an unphysical flame.

When the coflow is not hot enough to allow for an autoignition stabilized flame, another stabilizing mechanism must exist for a turbulent jet flame to exist. Two plausible flame stabilization mechanisms are considered for the H_2-N_2 turbulent jet flames in a vitiated coflow, namely autoignition and flame propagation. A 1-D RANS parabolic model simulates experimentally determined regions or regimes of stability for conditions generating a lifted jet flame. Numerical results for the attached, lifted, and lifted-unsteady regimes show that the correct trend is captured, when compared with experimental results. At low coflow equivalence ratios (i.e. below the autoignition temperature), turbulent flame propagation is believed the main mechanism as the autoignition delay time is too large to stabilize a flame. At higher coflow equivalence ratios (i.e. where the autoignition temperature is reached), autoignition is believed the main mechanism as the minimum autoignition delay time decreases by several orders of magnitude. Typically, hydrogen jet flames require a diluent, such as nitrogen, to lift from the nozzle. By increasing the N_2 content in fuel, the jet momentum also increases, but by doing so slows down turbulent flame speed. Thus, as

N_2 content in fuel increases, the local turbulent mean axial velocity ($\bar{U}$) eventually blows out the flame.

The ability to accurately predict turbulent lifted hydrogen jet flames in a large scale code (such as LES or RANS) requires the inclusion of differential diffusion effects as well as mechanisms to allow both flame propagation and autoignition. Not only do a wide range of τ_{ign} exist for the pressures and coflow compositions considered, but flame propagation adds another layer of complexity. Current large scale models typically do not allow (or do not capture well) both possible flame mechanisms. In fact, models are typically developed to solve either a premixed system or non-premixed system and thus a partially premixed system such as a lifted flame, presents many challenges as outlined in *Peters* [2000]. However, one possible solution is an extension of Flamelet Generated Manifolds (FGM) [*Nguyen et al.*, 2010]. Flamelet-Generated Manifolds were proposed to overcome the computational limitations encountered by the transient flamelet model. Meaning, instead of solving for a full set of species equations in the typical transient flamelet model (expensive to do so in RANS or LES), a reaction progress variable, C, is used as an additional parameter. The source of the progress variables can be tabulated as (ξ, C, χ_z) for non-premixed flames. The coupling of FGM to LES has been restricted to premixed or non-premixed flames with promising results [*Nguyen et al.*, 2010; *Lodier et al.*, 2011]. For many applications, including a lifted jet flame, a more general approach for simulating multiple regimes is desirable as practical applications generally are not limited to one flame regime. A method to extend the FGM to multi-regime applications has been proposed and named Multidimensional Flamelet generated Manifold (MFM). This new formulation was derived from first principles with selected hypotheses. Chemical sources and properties are tabulated by five key parameters $(\xi, C, \chi_z, \chi_c, \chi_{zc})$. So far MFM has been evaluated for multi-regime laminar cases, which show promising results [*Knudsen & Pitsch*, 2012].

Bibliography

Caldeira, K.; M. Wickett, Anthropogenic carbon and ocean pH, *Nature* 425 (6956): 365365 (2003).

Cabra, R., Turbulent Jet Flames in a Vitiated Coflow, University of California Berkeley, Doctoral Dissertation, (2003).

Cabra, R., T. Myhrvold, J. Y. Chen, R. W. Dibble, A. N. Karpetis, and R. S. Barlow, Simultaneous laser Raman-Rayleigh-LIF measurements and numerical modeling results of a lifted turbulent H2/N2 jet flame in a vitiated coflow, *Proceedings of the Combustion Institute*, 29, 1881-1888 (2002).

Chen, J. Y., and W. Kollmann, PDF modeling of chemical nonequilibrium effects in turbulent nonpremixed hydrocarbon flames, *Symposium (International) on Combustion*, 22, 645-653 (1989).

Chen, J. Y., and W. C. Chang, Modeling differential diffusion effects in turbulent nonreacting/reacting jets with stochastic mixing models, *Combustion Science and Technology*, 133, 343-375 (1999).

Frederick, D. J. Design of a Vitiated Coflow Burner for Elevated Pressure Experiments, University of California Berkeley, Masters Thesis, (2010).

Hilbert, R., and D. Thévenin, Autoignition of turbulent non-premixed flames investigated using direct numerical simulations, *Combustion and Flame*, 128, 22-37 (2002).

Im, H.G., J.H. Chen, and C.K. Law, Ignition of hydrogen-air mixing layer in turbulent flows, *Symposium (International) on Combustion*, 27, 1047-1056 (1998).

Metz, B., O. Davidson, H. C. de Coninck, M. Loos, and L.A. Meyer (eds.), IPCC special report on Carbon Dioxide Capture and Storage. *Cambridge University Press, Cambridge, United Kingdom and New York, NY, USA* (2005).

Jacobs, D., An Introduction to Atmospheric Chemistry, 129. Princeton University Press, New Jersey, U.S.A., (1999).

Kee, R., J. Grcar, M. Smoooke, and J. Miller, Premix: A fortran program for modeling steady laminar one-dimensional premixed flames, *Sandia Report*, SAND 87-8240 (1985).

Kernstein, A. R., A Linear-Eddy model of turbulent scalar transport and mixing, *Combustion Science and Technology*, 60(4), 391-421 (1988).

Kernstein, A. R., Pair-exchange model of turbulent premixed flame propagation, *Symposium (International) on Combustion*, 21(1), 1281-1289 (1988).

Kernstein, A. R., Linear-Eddy modeling of turbulent transport. Part 6: Microstructure of diffusive scalar mixing fields, *Journal of fluid Mechanics*, 261, 361-394 (1991).

Knikker, R., A. Dauptain, B. Cuenot, and T. Poinsot, Comparison of computational methodologies for ignition of diffusion layers, *Combustion Science and Technology*, 175, 1783-1806 (2003).

Knudsen, E., H. Pitsch, Capabilities and limitations of multi-regime flamelet combustion models, *Combustion and Flame*, 159, 242-264 (2012).

Li, J., Z. Zhao, A. Kazakov, F.L. Dryer, An updated comprehensive kinetic model of hydrogen combustion, *International Journal of Chemical Kinetics*, 36, 566-575 (2004).

Lodier, G., L. Vervisch, V. Moureau, P. Domingo, Composition-space premixed flamelet solution with differential diffusion for in situ flamelet-generated manifolds, *Combustion and Flame*, 158, 2009-2016 (2011).

Lutz, A. E., R. J. Kee, and J. A. Miller, Senkin: A fortran program for predicting homogeneous gas phase chemical kinetics with sensitivity analysis, *Sandia Report*, SAND 87-8248 (1988).

Mastorakos, E., T. A. Baritaud, T. J. Poinsot, Numerical simulations of autoignition in turbulent mixing flows, *Combustion and Flame*, 109, 198-223 (1997).

Mastorakos, E., Ignition of turbulent non-premixed flames, *Progress in Energy and Combustion Science*, 35, 57-97 (2009).

McMurty, P. A., S. Menon, A.R. Kerstein, Linear Eddy Modeling of Turbulent Combustion, *Energy and Fuels*, 7, 817-826 (1993).

Muppala, S., J. X. Wen, N. K. Aluri, F. Dinkelacker, Molecular Transport Effects of Hydrocarbon Addition on Turbulent Hydrogen Flame Propagation, 2nd International Conference on Hydrogen Safety, EU NoE HySafe, San Sebastian, ES, (2007).

Nguyen, Phuc-Danh, L. Vervisch, V. Subramanian, P. Domingo, Multidimensional flamelet-generated manifolds for partially premixed combustion, *Combustion and Flame*, 175, 43-61, (2010).

North, A., Experimental Investigations of Partially Premixed Hydrogen Combustion in Gas Turbine Environments, University of California Berkeley, Doctoral Dissertation, (2013).

Patnaik P., A Comprehensive Guide to the Hazardous Properties of Chemical Substances, Wiley-Interscience, Hoboken, New Jersey, U.S., 402, (2007).

Peters, N., Turbulent Combustion, Cambridge University Press, (2000).

Pope, S. B., Monte Carlo method for the PDF equations of turbulent reactive flow, *Combustion Science and Technology*, 25, 159. (1981).

Pope, S. B., Computations of Turbulent Combustion: Progress and Challenges, *Invited Plenary Lecture, Proceedings from the 23rd International Symposium on Combustion*, The Combustion Institute, Pittsburgh, 591-612 (1990).

Pope, S. B., Turbulent Flows, Cambridge University Press, (2000).

Pitsch, H., N. Peters, Unsteady flamelet modeling of turbulent hydrogen-air diffusion flames, *Proceedings from the 27th International Symposium on Combustion*, The Combustion Institute, Pittsburgh, 1057-1064 (1998).

Pitsch, H., N. Peters, A consistent flamelet formulation for non-premixed combustion considering differential diffusion effects, *Combustion and Flame*, 114, 26-40 (1998).

Sung, C. J.., C. K. Law, J. Y. Chen, An augmented reduced mechanism for methane oxidation with comprehensive global parametric validation, *Proceedings of the Combustion Institute*, 27, 295-304 (1998).

Smith, N.S.A., Bilger, R.W., Carter, C.D., Barlow R.S., & Chen, J.-Y., A Comparison of CMC and PDF Modelling Predictions with Experimental Nictroic Oxide LIF/Raman Measurements in a Turbulent H_2 Jet Flame, *Combustion Science and Technology*, 105, 357-375 (1995).

Smith, T., S. Menon, One-dimensional Simulations of Freely Propagating Turbulent Premixed Flames, *Combustion Science and Technology*, 128, 99-130 (1997).

Sreedhara, S., and K.N. Lakshmisha, Autoignition in a non-premixed medium: DNS studies on the effects of three-dimensional turbulence, *Proceedings of the Combustion Institute*, 29, 2051-2059 (2002).

United States Environmental Protection Agency, Inventory of U.S. Greenhouse Gas Emissions and Sinks: 1990 - 2011, *EPA 430-R-13-001*, Retrieved from http://www.epa.gov/climatechange/ghgemissions/usinventoryreport.html, (2013).

Warnatz, J., U. Maas, and R. W. Dibble, Combustion, 127. Springer, Germany (2006).

Yetter, R., F. Dryer, H. Rabitz, A comprehensive reaction mechanism for carbon monoxide/hydrogen/oxygen kinetics, *Combustion Science and Technology*, 79, 97-128 (1991).